12768 *Biochemistry* **1999,** *38,* 12768−12785

Component Interactions in the Soluble Methane Monooxygenase System from *Methylococcus capsulatus* (Bath)[†]

George T. Gassner and Stephen J. Lippard*

Department of Chemistry, Massachusetts Institute of Technology, Cambridge, Massachusetts 02139

Received April 9, 1999; Revised Manuscript Received June 15, 1999

ABSTRACT: The soluble methane monooxygenase system of *Methylococcus capsulatus* (Bath) includes three protein components: a 251-kDa non-heme dinuclear iron hydroxylase (MMOH), a 39-kDa iron−sulfur- and FAD-containing reductase (MMOR), and a 16-kDa regulatory protein (MMOB). The thermodynamic stability and kinetics of formation of complexes between oxidized MMOH and MMOB or MMOR were measured by isothermal titration calorimetry and stopped-flow fluorescence spectroscopy at temperatures ranging from 3.3 to 45 °C. The results, in conjunction with data from equilibrium analytical ultracentrifugation studies of MMOR and MMOB, indicate that free MMOR and MMOB exist as monomers in solution and bind MMOH with 2:1 stoichiometry. The role of component interactions in the catalytic mechanism of sMMO was investigated through simultaneous measurement of oxidase and hydroxylase activities as a function of varied protein component concentrations during steady-state turnover. The partitioning of oxidase and hydroxylase activities of sMMO is highly dependent on both the MMOR concentration and the nature of the organic substrate. In particular, NADH oxidation is significantly uncoupled from methane hydroxylation at MMOR concentrations exceeding 20% of the hydroxylase concentration but remains tightly coupled to propylene epoxidation at MMOR concentrations ranging up to the MMOH concentration. The steady-state kinetic data were fit to numerical simulations of models that include both the oxidase activities of free MMOR and of MMOH/MMOR complexes and the hydroxylase activity of MMOH/MMOB complexes. The data were well described by a model in which MMOR and MMOB bind noncompetitively at distinct interacting sites on the hydroxylase. MMOB manifests its regulatory effects by differentially accelerating intermolecular electron transfer from MMOR to MMOH containing bound substrate and product in a manner consistent with its activating and inhibitory effects on the hydroxylase.

The first step in the carbon assimilation pathway of methanotrophs is the oxidation of methane to methanol by soluble or membrane-bound methane monooxygenases (*1*, *2*). The sMMO[1] systems from two such organisms, *Methylococcus capsulatus* (Bath) (*3*, *4*) and *Methylosinus trichosporium* OB3b (*5*, *6*) have been purified and extensively investigated. Both systems have three components, a dimeric $(\alpha\beta\gamma)_2$ hydroxylase (MMOH) containing two carboxylate-bridged dinuclear iron centers, a NADH-dependent [2Fe-2S] and FAD-containing reductase (MMOR), and a small regulatory protein (MMOB). These enzyme systems can hydroxylate a broad spectrum of organic compounds in addition to methane, making them potentially useful for aqueous-phase organic synthesis (*7*). They are of additional value for decontaminating regions in the environment that are polluted with toxic wastes such as chlorinated ethylenes that accumulate in ground water as byproducts of industrial processes (*8*). The ability of methane monooxygenases to convert methane selectively to methanol under ambient conditions, which has yet to be duplicated with synthetic analogues (*9*, *10*), has further stimulated interest in the details of their catalytic mechanism.

The rate and catalytic efficiency of sMMO systems is highly dependent on the relative concentrations of MMOH, MMOR, and MMOB present in the reaction mixture (*11*−*14*). Three substrates are involved in the reaction of sMMO. Both O_2 and CH_4 react at the dinuclear iron centers of MMOH, whereas the third, NADH, reacts at the FAD center of MMOR. Steady-state kinetic data support a catalytic cycle in which the sMMO system reacts sequentially with CH_4, NADH, and O_2 (*15*). Initially, methane binds to the oxidized hydroxylase. NADH subsequently transfers a hydride to the FAD moiety of MMOR, and two electrons are transmitted sequentially from the reduced FAD through the [2Fe-2S] center of MMOR to a diiron(III) center of the hydroxylase by means of intra- and intermolecular electron-transfer reactions (*11*, *16*). Molecular oxygen then binds to the diiron(II) center of the hydroxylase where it is reductively activated to hydroxylate methane, forming methanol and water (*17*, *18*).

[†] This work was supported by Grant GM 32134 from the National Institutes of Health General Medical Sciences. G.T.G. is an NIH postdoctoral fellow.

* Author to whom correspondence should be addressed.

[1] Abbreviations: sMMO (Bath) or (OB3b), soluble methane monooxygenase systems from *Methylococcus capsulatus* (Bath) or *Methylosinus trichosporium* OB3b, respectively; H_{ox}, H_{mv}, H_{peroxo}, and Q, methane monooxygenase hydroxylase oxidized, mixed-valent, peroxo, and Q species, respectively; MMOB, methane monooxygenase coupling protein; MMOR, methane monooxygenase reductase; FAD, flavin adenine dinucleotide; NAD(H), nicotinamide adenine dinucleotide (reduced form); ITC, isothermal titration calorimetry; DCPIP, dichlorophenolindophenol.

10.1021/bi990841m CCC: $18.00

The regulatory protein MMOB directs the outcome of both the oxidative and reductive half-reactions of MMOH. In the presence or absence of MMOB, MMOR transfers electrons to the diiron(III) center of MMOH; the resulting H_{red} binds and reduces molecular oxygen. In the absence of MMOB, the intermediates necessary for methane hydroxylation do not accumulate and dioxygen bound at the active site is reduced to water (*11*).

Despite the substantial body of evidence for interactions among the sMMO component proteins, there is little information about complex formation. Here we present new thermodynamic and kinetic data for component interactions in the sMMO system from *M. capsulatus* (Bath) and compare catalytic mechanisms that are most consistent with these results.

EXPERIMENTAL PROCEDURES

Purification of MMOH. By using a protocol very similar to one reported for *M. trichosporium* OB3b (*5*), preparations of the sMMO (Bath) hydroxylase with specific activities in the range of 350−400 milliunits/mg were routinely obtained. Typically, 100 g of cell paste resuspended in cell disruption buffer (100 mL) was sonicated in five 3-min cycles at 40% maximum power with a Branson model 450 sonicator fitted with a $^3/_4$-in horn. The temperature was maintained below 10 °C by cooling the cells in an ice/ethanol slush during sonication. The cell disruption buffer contained 25 mM MOPS (pH 7.0), 8 mM sodium thioglycolate, 2 mM cysteine, 200 μM ferrous ammonium sulfate, 5 mM $MgCl_2$, DNase (1.5 units/mL), and 1 mM each of Pefabloc SC (Boehringer Mannheim) and phenylmethanesulfonyl fluoride (PMSF). Cellular debris was pelleted by ultracentrifugation for 35 min at 100000*g* in a Beckman model L-70 ultracentrifuge. The supernatant was filtered through a 0.22-μm membrane and loaded onto a 5 × 50 cm DEAE-Sepharose fast-flow column that was equilibrated in 25 mM MOPS (pH 7.0) containing 8 mM sodium thioglycolate, 2 mM cysteine, and 200 μM ferrous ammonium sulfate (buffer A). After the sample was loaded, the column was washed with 1 L of buffer A followed by a linear 4.3-L gradient of 0−400 mM NaCl in the same buffer. The hydroxylase eluted from the column at approximately 160 mM NaCl. Hydroxylase-containing fractions were identified by absorbance at 280 nm, activity, and SDS−PAGE assays. Pooled fractions were concentrated over a 72 mm YM-100 Amicon membrane. Between 20 and 50 mg of the concentrated protein was loaded onto a 2.5 cm × 1 m S-300 size-exclusion column equilibrated in buffer A containing 1 mM DTT, 5% glycerol, and 120 mM NaCl. Fractions were assayed for activity by combining 100 μL aliquots with the other components and substrates to give final concentrations of 200 nM MMOR, 1 μM MMOB, 160 μM NADH, and 1 mM propylene in a final volume of 400 μL of 25 mM MOPS buffer (pH 7) at 25 °C. Reaction rates were calculated from the change in absorbance at 340 nm as a function of time. Fractions having a ratio of activity to absorbance at 280 nm >10% of the maximum value were pooled.

Purification of MMOB. MMOB is quite susceptible to proteolytic cleavage (*19*, *20*); as a consequence, it is not possible to recover homogeneous preparations of MMOB from *M. capsulatus* (Bath). Intact MMOB can be purified from a recombinant *Escherichia coli* expression system, however (*21*). Initially, the protein was purified following published procedures for native MMOB (*22*). In this preparation, MMOB in the cell extract was precipitated with ammonium sulfate and subsequently purified by Sephadex G-50 gel-filtration, Q-Sepharose anion-exchange, and hydroxyapatite chromotography. A significant amount of MMOB was lost in the ammonium sulfate precipitation step, however. Since contaminating proteins removed by this procedure were equally well separated in the subsequent chromatography steps, the ammonium sulfate precipitation step was discontinued. It has been reported that proteolytically truncated MMOB could be resolved from intact MMOB by hydroxyapatite chromatography (22). We could not reproduce this separation, however, and this chromatographic step could be eliminated with no significant loss of sample purity. Good results were obtained with 25 mM MOPS (pH 6.5) containing 1 mM EDTA. The chromatographic resolution was further improved by substituting a 2.5 × 25 cm DEAE CL6B column for the Q-Sepharose column and a 2.5 cm × 1.2 m Bio-Gel P-60 column for the Sephadex G-50 column used in the original preparation.

Purification of Methane Monooxygenase Reductase. Although it is possible to isolate routinely high-quality MMOR from *M. capsulatus* (Bath), only relatively small quantities are obtained from such preparations. Typically, 6−10 mg of highly purified protein can be recovered from 100 g of cell paste. By use of a recombinant *E. coli* system that overexpresses MMOR, 100−150 mg of pure MMOR can be isolated from a 10-L preparation following DEAE anion-exchange and 5′-AMP affinity chromatography. The plasmid construction and details of the purification will be described elsewhere (*23*).

Amino Acid Analysis. Purified samples of each sMMO component were submitted to the Harvard Biopolymer Laboratory in triplicate for total amino acid analysis. Optical spectra were recorded by using an HP8452 diode-array spectrophotometer to determine accurate absorbance values. Samples were hydrolyzed in 6 N HCl for 22 h, resolved by anion-exchange HPLC, and detected after postcolumn derivatization with ninhydrin. Peak areas corresponding to sMMO hydrolysates were compared with those of amino acid standards so that molar concentrations of the amino acids could be calculated. In all cases, the relative amounts of amino acids detected in hydrolysates were in excellent agreement with the ratios predicted from the known primary gene sequences of the sMMO components.

Equilibrium Binding Measurements. A Beckman Optima series XL-A analytical ultracentrifuge was used to determine the self-association state of MMOR and MMOB. Data from these studies were recorded and processed with Origin v. 3.5 software (MicroCal Software Inc., North Hampton, MA). An Omega model isothermal titration calorimeter (MicroCal, Inc., Northampton, MA) was used to estimate binding affinities and stoichiometries of protein−protein complexes. Titration data were recorded over a range of temperatures in 25 mM TRIS, pH 7.0 buffer containing 1 mM DTT. No significant difference in binding enthalpy was detected when Tris buffer was substituted for MOPS buffer. Samples containing 5−15 μM MMOH were equilibrated for 20−30 min at the reaction temperature prior to introduction to the instrument. Titrant (250−300 μM MMOB or MMOR) was delivered in aliquots from a 100-μL stirred titration syringe into the 1.341-mL active cell volume of the calorimeter. Samples were routinely stirred at 350 rpm during titrations. Data were integrated and used to construct binding isotherms, which were fit with the Origin software package (MicroCal, Inc.) or simulated by using the program KaleidaGraph v 3.0 (Synergy Software).

Kinetic Measurements. Reactions were performed in 25 mM MOPS or phosphate buffer at pH 7.0. Steady-state kinetic data were recorded at 10 Hz by using an HP8452 diode array spectrophotometer. Temperature was controlled in the range 4−45 °C with a NesLab RTE-140 circulating water bath. The consumption of NADH was monitored spectrophotometrically at 340 nm and quantified by using an extinction coefficient of 6.22 $\mathrm{mM}^{-1}\ \mathrm{cm}^{-1}$.

A Hewlett−Packard 5890 gas chromatograph was used to detect propylene and propylene oxide in MMO reaction mixtures. Samples (200 μL) were quenched and extracted with 50 μL of chloroform and then centrifuged for 5 min to separate the aqueous and organic phases. Aliquots (5 μL) of the chloroform phase were injected onto a Deactiglas Porapak Q column maintained at 160 °C. Peaks corresponding to propylene and propylene oxide were integrated and quantified by comparison to standard curves obtained with the pure compounds.

Methanol production by the sMMO system was measured discontinuously in a coupled enzymatic assay. Reaction sample volumes of 600 μL containing 25 mM pH 7.0 potassium phosphate buffer were acidified with 50 μL of 1 M HCl. After 5 min, samples were neutralized with 50 μL of 1 M NaOH and brought to pH 7.5 by addition of 67 μL of 1 M potassium phosphate buffer. Denatured protein was removed by centrifugation. A 600-μL aliquot of quenched sample was combined with 20 μL of a 1 mg/mL solution of alcohol oxidase from *Candida boidinii* (EC 1.1.3.13) and 50 μL of a 1 mg/mL solution of formaldehyde dehydrogenase from *Pseudomonas putida* (EC 1.2.1.46) obtained from Sigma (St. Louis, MO). After NAD^+ was added to a concentration of 1 mM, the initial rate of NADH production was measured spectrophotometrically at 340 nm. Both the rate and total amount of NADH produced were directly related to the amount of methanol in solution. Methanol concentrations as low as 5 μM could be measured accurately by comparison to standards of known concentration.

Hydrogen peroxide was detected colorimetrically by measuring the absorbance of the colored ferric thiocyanate complex that developed after reacting acid-quenched samples with ferrous ammonium sulfate and sodium thiocyanate (*24*).

Protein−protein complex formation was detected by monitoring the quenching of intrinsic tryptophan fluorescence in static titrations and stopped-flow experiments. In the titration experiments, samples were excited with 280 nm light and fluorescence emission was recorded at 360 nm. Fluorescence was excited along the short axis, and emission was monitored along the long axis, of a 4 mm × 10 mm fused silica cuvette. A significant inner filter effect (*25*) was observed when MMOH was titrated with MMOR concentrations exceeding 3 μM and MMOB concentrations greater than 4 μM. When enzyme concentrations were kept below these values, significant quenching of tryptophan fluorescence was observed in titrations of MMOH with MMOB or MMOR. There was no evidence for fluorescence quenching in titrations of MMOR with MMOB in the sMMO (Bath) system, although it has been reported for the corresponding proteins in the sMMO (OB3b) system (*26*). Data recorded in static titrations were deemed unreliable due to photochemical reactions of the individual MMOB and MMOH components, which occur upon exposure to 280 nm light. These reactions were characterized by a slow, nonlinear increase in the fluorescence of MMOH and a decrease in MMOB fluorescence. Since these photochemical reactions were slow on the time scale of the binding reaction, the kinetics of complex formation could be monitored by stopped-flow fluorescence spectroscopy. The data were recorded by using a Hi-Tech DX-2 stopped-flow spectrophotometer with a 2 ms dead time. Samples were excited with 280 nm light and a 320 nm cutoff filter was used to prevent stray light from entering the emission photomultiplier.

Time-resolved absorbance measurements of intra- and intermolecular electron-transfer reactions in the sMMO system were recorded by using the Hi-Tech DX-2 stopped-flow instrument configured for either single-wavelength photomultiplier or multiwavelength diode-array data collection. Diode-array data were recorded with a 1.25 ms integration time. All data were recorded with a logarithmic time base.

Single-wavelength fluorescence and absorbance data from stopped-flow studies were fit with the program KinetAssyst v 2.0 (Hi-Tech Ltd.), and multiwavelength diode-array data were fit with the program Specfit v 2.10M. Steady-state kinetic data were simulated and fit by using the programs KaleidaGraph v 3.0 (Synergy Software) and HopKINSIM, version 1.7 for Macintosh adapted from the KINSIM program (*27*, *28*). Initially, the model-dependent equilibrium distribution of species was simulated as a function of varied component concentrations. The resulting concentration tables were then referenced in least-squares fits of the steady-state data to obtain the best estimates of velocity parameters for the tested models.

RESULTS

Extinction Coefficients of sMMO Component Proteins. Extinction coefficients were previously calculated on the basis of aromatic amino acid and cysteine content or protein dry weight (*29*, *30*). Subsequently, several errors were identified in the reported primary gene sequences of all three MMO components (*23*, *31*). Extinction coefficients were redetermined with increased accuracy by calculating the protein concentration from the amino acid analysis of purified samples. Based on this calculation, ϵ_{280}(MMOH) = 664 760 ± 3 589 $\mathrm{M}^{-1}\ \mathrm{cm}^{-1}$, ϵ_{458} (MMOR) = 20 828 ± 2 233 $\mathrm{M}^{-1}\ \mathrm{cm}^{-1}$, and ϵ_{280}(MMOB) = 19 256 ± 784 $\mathrm{M}^{-1}\ \mathrm{cm}^{-1}$. The extinction coefficient of the hydroxylase reported here is bracketed by the previously accepted value of 567 200 $\mathrm{M}^{-1}\ \mathrm{cm}^{-1}$, based on amino acid content (*29*, *30*), and the value of 788 400 $\mathrm{M}^{-1}\ \mathrm{cm}^{-1}$, which was based on protein dry weight (*29*). The MMOR extinction coefficient at 458 nm reported here is consistent with its iron−sulfur and FAD content and is in very good agreement with a previously reported value of 21 200 $\mathrm{M}^{-1}\ \mathrm{cm}^{-1}$ (*32*). The extinction coefficient calculated for MMOB of 19 180 $\mathrm{M}^{-1}\ \mathrm{cm}^{-1}$ at 280 nm (*29*) is also in excellent agreement with the value determined here by amino acid analysis.

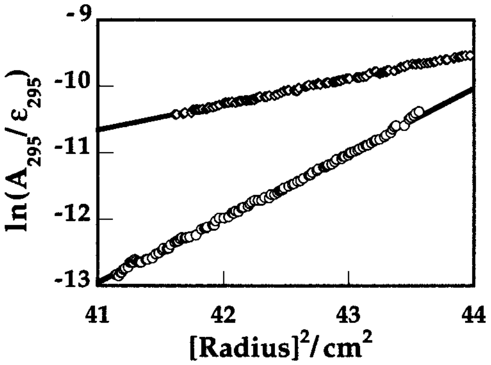

FIGURE 1: Aggregation of protein components in the sMMO (Bath) system. Analytical ultracentrifugation data recording the sedimentation equilibria of (◇) 69.7 μM MMOB and (○) 9.7 μM MMOR are shown. Data were recorded after 18.6 h of centrifugation at 25 °C. Plots of ln [protein] vs (radial distance)^2 were used to calculate protein component molecular weights according to eq 1.

Aggregation State of MMOR and MMOB. The possibility that MMOB and related proteins may exist as a dimer in solution has been suggested on the basis of covalent cross-linking and gel-filtration studies (*26*, *33*). Solution NMR studies of MMOB from *M. trichosporium* OB3b suggest that, at concentrations greater than 200 μM MMOB, dimers may form (*34*). No significant enthalpy of dissociation could be detected, however, when MMOB from *M. capsulatus* (Bath) was diluted in the isothermal titration calorimeter. Moreover, it has been shown through analysis of analytical gel-filtration studies that MMOB from *M. capsulatus* (Bath) migrates anomalously as a dimer independent of protein concentration (*20*). To resolve these apparently contradictory findings and to confirm the proposed monomeric structure of MMOR, each enzyme was subjected to equilibrium analytical ultracentrifugation. This measurement depends only on partial specific volume of the investigated molecule and the applied centripetal force (*35*). As a result, equilibrium ultracentrifugation is insensitive to differences in molecular shape, which may lead to anomalous behavior in gel-permeation studies. Specific volumes of MMOB and MMOR were calculated on the basis of their amino acid compositions to be 0.7355 g/mL for MMOB and 0.7313 g/mL for MMOR (*36*). Rotor speed and sample concentrations were varied to find optimal conditions. Excellent results were obtained with 2094 rad/s with sample concentrations of 69.7 μM MMOR and 9.7 μM MMOB. Sample equilibrium was reached after 16 h. The protein concentration gradient that develops at equilibrium is described by eq 1 (*35*, *37*), where C is the protein

$$\mathrm{d}\,(\ln C) = [(1 - \rho\nu)M_\mathrm{r}\omega^2/RT]\,\mathrm{d}r^2 \qquad (1)$$

concentration, ρ is the solution density, ν is the specific volume of the protein, M_r is the molecular weight, ω is the angular velocity, r is the radius, R is the gas constant, and T is the absolute temperature. From this relationship, we calculated molecular mass values of 15.9 kDa for MMOB and 39.9 kDa for MMOR from the slopes of the best-fit lines through plots of ln C vs r^2 (Figure 1). These values are consistent with monomeric structures for these proteins.

Protein Complexes Formed by sMMO. It was previously reported that MMOR and MMOB isolated from *M. trichosporium* OB3b associate and form a stable complex (*26*). We find no evidence to support this possibility in the sMMO system from *M. capsulatus* (Bath). No significant quenching or enhancement of tryptophan fluorescence was observed in titrations of MMOR with MMOB. In addition, no significant change in enthalpy was detected by isothermal titration calorimetry when MMOR was titrated with MMOB. Finally, MMOB had no effect on the NADH oxidase or DCPIP diaphorase activities of MMOR. On this basis, we conclude that the MMOB/MMOR complex does not form in the sMMO system from *M. capsulatus* (Bath). On the other hand, we have strong thermodynamic and kinetic evidence for complexes formed by MMOH with MMOR or MMOB.

Data from isothermal titration calorimetry studies are presented in Figure 2. Plots shown in Figure 2A,B record the power required to compensate for the heat absorbed or released in sequential additions of MMOB or MMOR to MMOH in the calorimeter cell. Numerical integration of the heat pulses in these plots over time gives the incremental heat change, Δq_i, for each step in the titration. Plots of these data as a function of MMOB/MMOH and MMOR/MMOH concentration ratios are given in Figure 2C,D.

For each injection of titrant, a volume, v_i, is displaced from the fixed cell volume, V_0, of the calorimeter. This volume displacement is accounted for in eq 2, which is built into

$$q_i = \sum_{i=1}^{n}[\Delta q_i/(1 + v_i/2V_0) - q_{i-1}] \qquad (2)$$

the Origin program and allows the total heat released, q_i, to be calculated at any point in the titration. The relationship between binding enthalpy and q_i depends on the model used to fit the binding data. Initial fits through these data suggested that more than one binding site exists for both MMOR and MMOB, and the 2-fold symmetry of the hydroxylase structure is most consistent with a 2:1 binding stoichiometry for each component. Possible arrangements of protein components in these complexes are illustrated in Scheme 1, where subunits of hydroxylase dimers are labeled α, β, and γ and MMOR and MMOB are designated by solid ellipses and open circles, respectively. The site occupancy calculated from ITC data fitting typically ranged from 0.6 to 0.8 MMOB or MMOR equiv. In order to evaluate the possibility that the calculated substoichiometric site occupancies might result from dilution error due to sample diffusion into and out of the titrator syringe during the course of the experiment, the syringe was filled with a concentrated DCPIP solution and stirred at 350 rpm in the calorimeter cell for a period of 70 min. An absorbance reading of the cell solution indicated that diffusion of titrant into the cell was insignificant in this time frame.

From the ITC data and other evidence discussed below, we conclude that on average only 60−80% of the hydroxylase participates in binding to the other protein components. After correction of the hydroxylase concentration for the nonbinding fraction, excellent fits through enthalpy data were obtained by using a model with two interacting sites (Figure 2C,D). This model assumes that MMOB and MMOR binding sites on the surface of the hydroxylase are initially equivalent and that the binding of MMOB or MMOR at one site changes the affinity for binding at the remaining MMOB or MMOR binding site. The binding partition function (*38*) for this

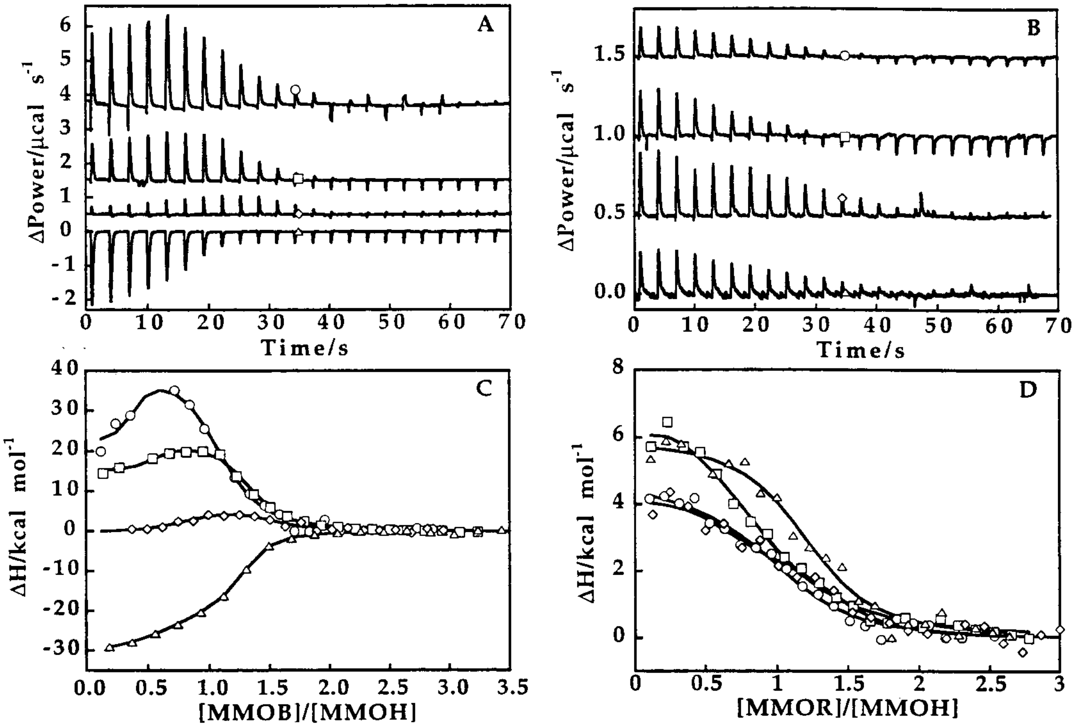

FIGURE 2: Isothermal titration calorimetry data recording complex formation between MMOH and (A) MMOB at (○) 16.6 °C, (□) 25.0 C, (◇) 34.8 °C, or (△) 45 °C and (B) MMOR at (○) 3.3 °C, (□) 10.0 °C, (◇) 18.7 °C, and (△) 25 °C. Sample concentrations ranged from 8 to 15 μM MMOH in the ITC cell and from 250 to 400 μM for MMOB or MMOR in the injection syringe. Each heat pulse corresponds to a 6 μL sample injection into the 1.341-mL cell volume of the calorimeter. After baseline subtraction to correct for the heat of dilution, data were incrementally offset for display purposes. Best fits through the integrated enthalpy in accord with the interacting sites model are given for the titrations of (C) MMOH with MMOB and (D) MMOH with MMOR.

Table 1: Thermodynamic Parameters from Protein Component Binding Interactions[a]

T (°C)	K_{d1} (μM)	ΔG_1 (kcal mol^{-1})	ΔH_1 (kcal mol^{-1})	$T\Delta S_1$ (kcal mol^{-1})	K_{d2} (μM)	ΔG_2 (kcal mol^{-1})	ΔH_2 (kcal mol^{-1})	$T\Delta S_2$ (kcal mol^{-1})
MMOH/MMOB								
10	1.6 (0.5)	−7.5	56.0	63.5	33.8 (7.2)	−5.8	12.9	18.7
17	0.1 (0.3)	−9.1 ± 0.7	24 ± 4	33 ± 30	0.2 (2.6)	−8.9 ± 0.6	57 ± 56	66 ± 55
25	0.3 (0.2)	−8.8 ± 0.5	18 ± 15	30 ± 14	0.7 (0.8)	−8.3 ± 0.4	19.5 ± 8.1	27.8 ± 8.0
35	0.04 (0.09)	−10.2 ± 0.7	5.0 ± 7.0	15 ± 6	0.1 (0.2)	−9.3 ± 1.0	3.5 ± 1.4	12.8 ± 2.4
45	0.10 (0.05)	−10.0 ± 0.7	−12.5 ± 5.0	17 ± 24	0.1 (0.06)	−9.8 ± 0.9	−19.3 ± 7.5	−9.5 ± 8.0
MMOH/MMOR								
3	0.4 (0.5)	−8.1	4.5	12.6	0.7 (1.0)	−7.8	2.4	10.1
10	1.0 (0.6)	−7.5 ± 0.1	3.6 ± 3.4	11.1 ± 3.5	1.7 (1.1)	−7.5 ± 0.2	6.3 ± 1.6	13.8 ± 1.4
19	0.2 (0.6)	−8.8 ± 0.5	4.0 ± 0.5	12.8 ± 0.1	0.4 (1.1)	−8.4 ± 0.4	16 ± 17	24 ± 17
25	0.9 (0.6)	−8.3	8.1	16.4	2.6 (1.1)	−7.6	6.5	14.1
35	0.5 (0.6)	−7.8 ± 0.3	6.4 ± 1.6	14.3 ± 1.2	0.6 (1.2)	−8.6 ± 0.5	4.6 ± 4.2	13 ± 5

[a] K_d values enclosed in parentheses were calculated from fits through van't Hoff plots of the data using eqs 1−4 given in the text.

model is given by eq 3, where K_1 and K_2 represent the

$$P = 1 + K_1x + K_1K_2x^2 \qquad (3)$$

binding constants at the two interacting sites and x is the concentration of free MMOB or MMOR. The first, second, and third terms in eq 3 represent the free, singly-bound, and doubly-bound forms of the hydroxylase, respectively. The fraction of hydroxylase in each state is then given by $\alpha_0 = 1/P$, $\alpha_1 = K_1x/P$, and $\alpha_2 = K_1K_2x^2/P$. The total heat of the binding reaction is the sum of the heat changes associated with the formation of each bound state of the hydroxylase, as given in eq 4, where M_t is the protein concentration in

$$q_i = M_tV_0(\alpha_1\Delta H_1 + \alpha_2\Delta H_2) \qquad (4)$$

the cell at the start of the titration, V_0 is the active cell volume, and ΔH_1 and ΔH_2 are the binding enthalpies for the high- and low-affinity sites. Thermodynamic constants calculated from interacting-site fits through the data in Figure 2C,D are given in Table 1, and plots of these data as a function of temperature are presented in Figure 3. The sign of the enthalpy change for MMOB/MMOH complex formation is negative at high temperature and positive at low temperature, indicating that MMOB/MMOH binding reactions are endothermic below 30 °C and exothermic at higher temperatures. The enthalpy change associated with MMOR binding to MMOH is positive and essentially temperature-independent. Equations 5−8 represent the best fits through van't Hoff plots of the equilibrium constants calculated from ITC studies (Table 1) and can be used to estimate K_d values

Scheme 1

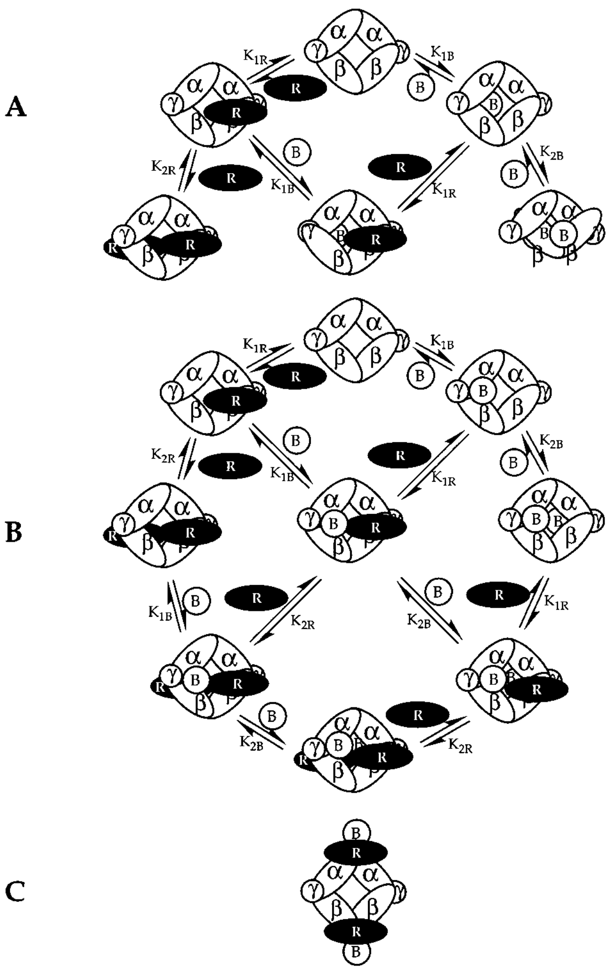

for the high- and low-affinity MMOB and MMOR binding sites at any temperature.

$$K_{d1}(B) = \exp(6282.5/T - 36.6) \quad (5)$$

$$K_{d2}(B) = \exp(12715.0/T - 56.7) \quad (6)$$

$$K_{d1}(R) = \exp(-484.4/T - 12.7) \quad (7)$$

$$K_{d2}(R) = \exp(-323.1/T - 12.6) \quad (8)$$

Steady-State Kinetic Studies. The role of protein component interactions during sMMO catalysis was investigated with NADH, molecular dioxygen, and either methane or propylene as substrates. Scheme 2 provides an overview of the reaction. Hydroxylase activity (Scheme 2A) is characterized by the reaction of the MMOH/MMOB complex with MMOR and substrates. The most efficient mode of catalysis is termed “coupled”, since only one molecule each of NADH and O_2 is consumed for each molecule of methanol or propylene oxide produced. Additional “uncoupled” modes of sMMO catalysis shown in Scheme 2 are discussed below.

The rates of NADH oxidation and propylene oxide or methanol production were simultaneously monitored during sMMO catalysis. The steady-state oxidase activities of MMOR and MMOH/MMOR complexes were investigated in the presence or absence of MMOB. For MMOR alone, consumption of NADH was coupled to the production of hydrogen peroxide (Table 2 and Scheme 2B). In reactions of MMOR with NADH and either MMOH or MMOH/MMOB complexes, NADH was consumed catalytically, but no hydrogen peroxide was formed (Table 2 and Scheme 2C). Finally, in the presence of hydrogen peroxide, protein component systems including MMOR and MMOH or MMOR, MMOH, and MMOB function as NADH peroxidases, consuming NADH and hydrogen peroxide in equal proportions (Table 2).

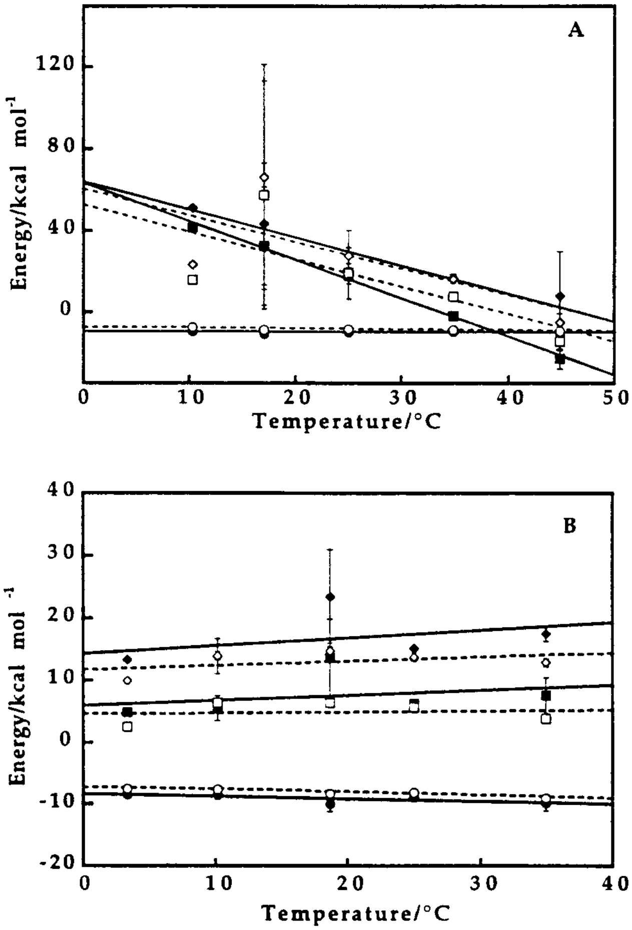

FIGURE 3: Linear fits through thermodynamic constants obtained from ITC titrations of MMOH with (A) MMOB and (B) MMOR. Temperature dependence of (circles) free energy, (squares) enthalpy, and (diamonds) entropy (plotted as $T\Delta S$) for the high-affinity (solid symbols) and low affinity (open symbols) MMOB binding sites. Error bars represent the standard deviation from the mean.

The steady-state behavior of sMMO as a function of protein component ratios and temperature is shown in Figure 4. As the MMOB to MMOH ratio increases, oxygenase activity increases to a maximum at 2 and then diminishes at higher ratios. The regulatory effects of MMOB are more pronounced at 45 °C, the optimum growth temperature for *M. capsulatus* (Bath), than at lower temperatures. Hyperbolic fits through these data give apparent K_d values for MMOB binding that decrease from 3.0 to 2.2 μM in the activation phase and from 4.3 to 2.7 μM in the inhibition phase of the reaction as temperature is increased from 4 to 45 °C. The apparent K_d value for MMOR binding increases from 110 to 370 nM over the same temperature range (Figure 4B). These steady-state kinetic trends are consistent with the temperature dependence of component binding measured by ITC (Table 1).

Scheme 2

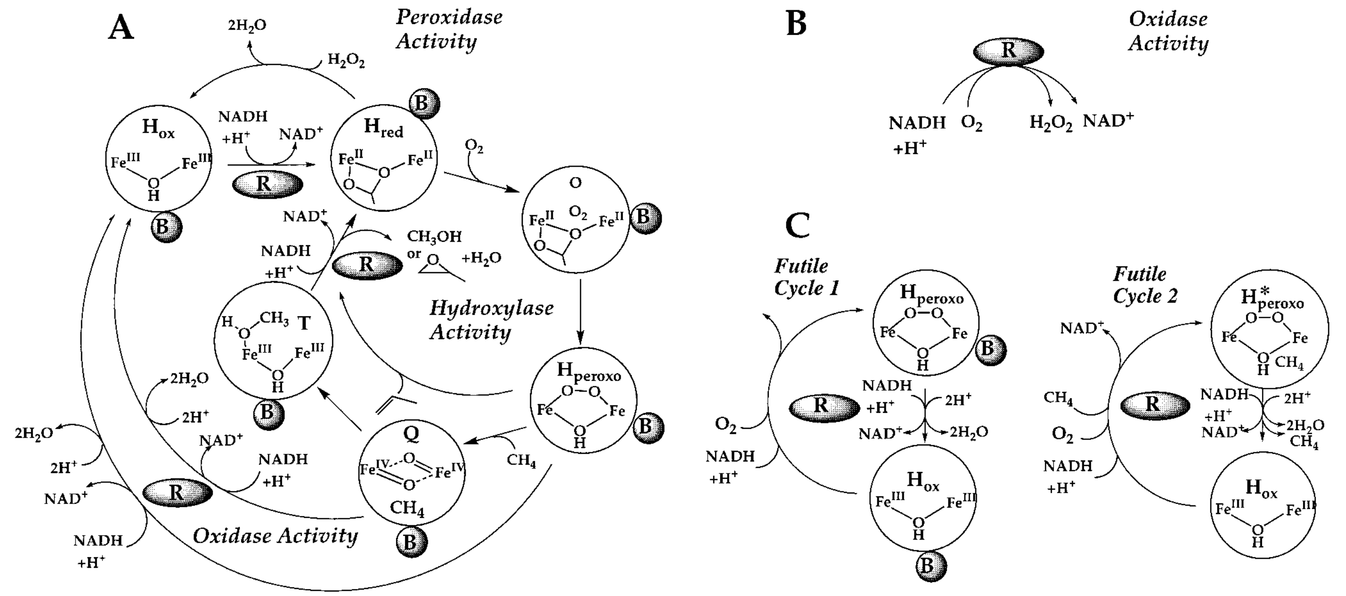

Table 2: Detection of Reduced Oxygen Species during Uncoupled Turnover Reactions of the MMO System

reaction components[a]	NADH (μM)	H_2O_2 (μM)	rate (NADH) (μM min^{-1})	rate (H_2O_2) (μM min^{-1})
MMOR +NADH	−9.4 ±1.1	+12.6 ±1.5	−0.9 ±0.1	+1.3 ±0.2
MMOR +MMOH +NADH	−66.2 ±7.9	< 1 ±0.8	−6.6	< 0.01
MMOR +MMOH +MMOB +NADH	−77.5 ±9.3	< 1 ±0.9	−7.7	< 0.01
MMOR +MMOH +MMOB +CH_4 +NADH	−72.5 ±8.7	<1 ±1.7	−14.2	< 0.01
MMOR +MMOH +MMOB +H_2O_2 +NADH	−77.4 ±9.3	−61.8 ±7.4	−7.6 ±0.9	−6.0 ±0.7

[a] Reactant concentrations were as follows: 200 μM NADH, 200 nM MMOR, 1 μM MMOB, 1 μM MMOH, 500 μM CH_4, 260 μM O_2, and 100 μM H_2O_2. NADH consumption was monitored continuously at 340 nm; H_2O_2 concentration was measured discontinuously after 300−600 s of reaction time.

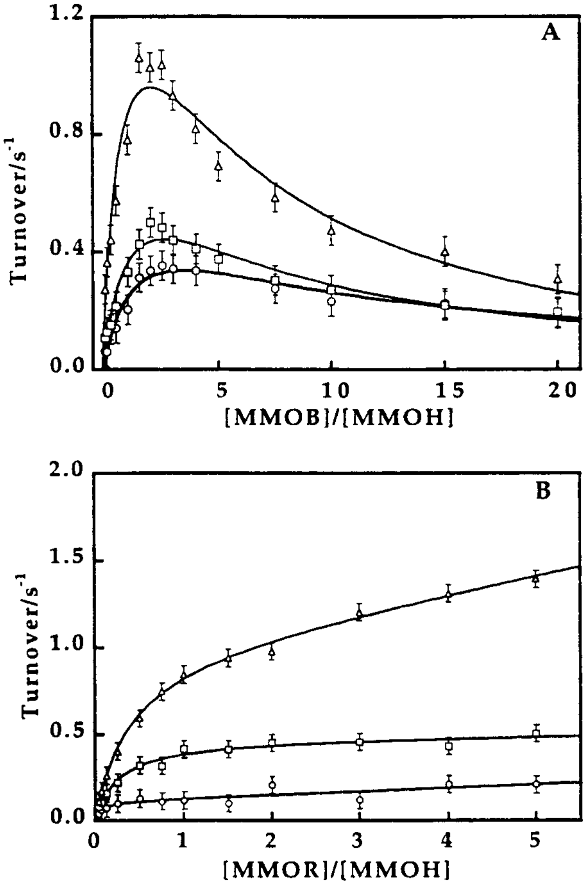

FIGURE 4: Temperature dependence of the protein concentration dependence of the steady-state methane oxidation reaction. Reacting solutions were air-saturated and contained 160 μM NADH and 100 μM methane at (○) 4 °C, (□) 25 °C, and (△) 45 °C. Fixed enzyme concentrations were (A) 2 μM MMOH and 0.4 μM MMOR and (B) 1 μM MMOH and 1 μM MMOB.

Two relatively simple models of steady-state catalysis that assume two MMOB and two MMOR binding sites per hydroxylase were evaluated. In the first model, MMOR and MMOB compete for binding sites. Protein complexes involved in this model are shown in Scheme 1A. The second model assumes that MMOR and MMOB bind noncompetitively. In this case, a maximum of two MMOR and two MMOB molecules can bind MMOH. Nine representative complexes are shown in Scheme 1B. Seven additional, symmetry-related complexes were included in the model used for data fitting to account for the statistical probability of binding all available sites on each hydroxylase molecule. Reaction rate constants for coupled hydroxylase activity were computed as being directly proportional to the fraction of the enzyme involved in complexes with both MMOB and MMOR. Rates of oxidase activity were computed as being proportional to the concentration of free MMOR and MMOH/MMOR$_n$ complexes. Catalytic rate constants were then calculated for the competitive and noncompetitive

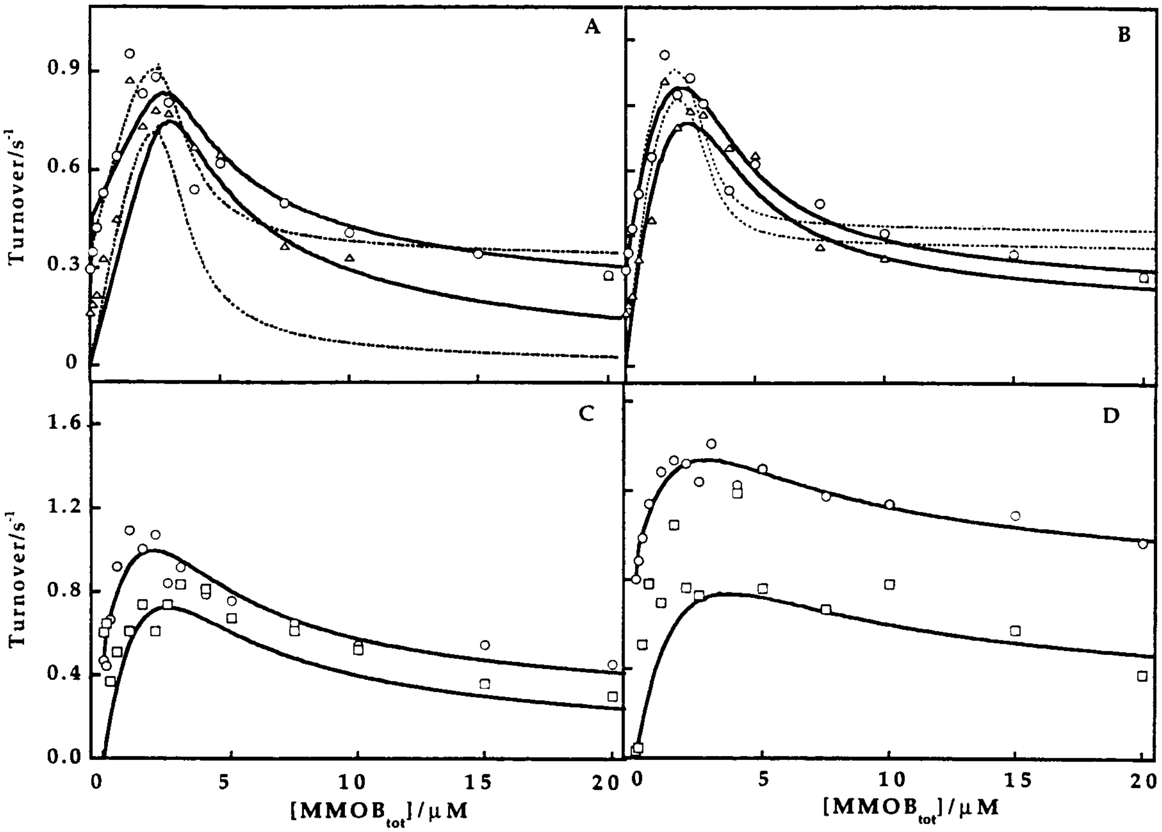

FIGURE 5: Comparison of fits of competitive and noncompetitive models to steady-state data from the reaction of the MMO system with methane at 45 °C (see Scheme 1 and text for details of models). Reactions including (A, B) 400 nM MMOR and 1.7 μM MMOH or 1 μM MMOH and (C) 1 μM MMOR or (D) 4 μM MMOR and various concentrations of MMOB were run in 25 mM phosphate buffer, pH 7, containing 0.1 mM DTT, 100 μM methane, 175 μLM O_2, and 160 μM NADH. Data corresponding to rates of NADH oxidation (○) and methanol production (□) are fit to (A) competitive and (B−D) noncompetitive models. Fits were calculated by using the following K_d values derived from ITC fits of MMOB and MMOR binding equilibria: (A) (···) ITC K_d values for both MMOB and MMOR, (—) ITC K_d values for MMOB, MMOR K_ds with 10 times higher affinity. Noncompetitive fits were calculated based on the basis of (B) (···) ITC K_d values, (—) ITC K_ds for MMOR, MMOB K_ds with 10-fold lower affinity; (C, D) ITC K_ds for MMOR, larger K_d values for MMOB as described in the text.

models by fitting kinetic data with eqs 9 and 10, respectively.

$$v^{c}_{(\text{oxidase + hydroxylase})} = \frac{[\mathrm{R}]k_{\mathrm{cat}}^{\ \mathrm{R}} + [\mathrm{HR}_n]k_{\mathrm{cat}}^{\ \mathrm{HR}_n} + [\mathrm{HRB}]k_{\mathrm{cat}}^{\ \mathrm{HRB}}}{[\mathrm{H}_{\mathrm{tot}}]} \quad (9)$$

$$v^{nc}_{(\text{oxidase + hydroxylase})} = ([\mathrm{R}]k_{\mathrm{cat}}^{\ \mathrm{R}} + [\mathrm{HR}_n]k_{\mathrm{cat}}^{\ \mathrm{HR}_n} + [\mathrm{HR}_n\mathrm{B}]k_{\mathrm{cat}}^{\ \mathrm{HR}_n\mathrm{B}} + [\mathrm{HR}_n\mathrm{B}_2]k_{\mathrm{cat}}^{\ \mathrm{HR}_n\mathrm{B}_2})/[\mathrm{H}_{\mathrm{tot}}] \quad (10)$$

In these equations the terms corresponding to concentrations of free enzyme species and complexes are bracketed. Hydroxylase molecules having one or more MMOR bound include the subscript *n*. Division in eqs 9 and 10 by H_{tot} results in reaction velocities that are turnover numbers with respect to the hydroxylase concentration. Oxidase activities are accounted for by the free reductase (R) term and by a term representing complexes of the hydroxylase and reductase (HR_n). Hydroxylase activities are represented by terms for the complexes, which include the hydroxylase bound to both the reductase and regulatory proteins. A related set of equations, which excludes terms in eqs 9 and 10 containing MMOB, was used to fit the oxidase activity of the sMMO system. In the model where MMOR and MMOB compete for sites on the hydroxylase, the observed inhibitory effect of MMOB can be explained by assuming that it sterically blocks the binding of MMOR and thus inhibits intermolecular electron transfer to MMOH. In the noncompetitive model, a more subtle effect must occur.

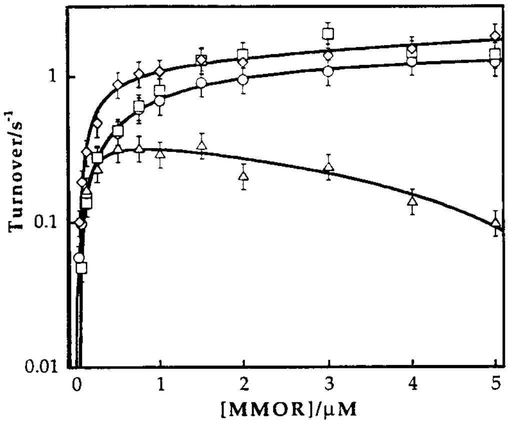

FIGURE 6: Differential catalytic efficiency of sMMO with methane and propylene as substrates. Solid lines depict fits through steady-state kinetic data from the reaction of 1 μM MMOH with 100 μM methane or propylene and 160 μM NADH at 45 °C in the presence of 1 μM MMOB and a range of MMOR concentrations. Rates of (△) methanol and (□) propylene oxide production are compared with rates of NADH consumption in reactions of MMO with (◇) methane and (○) propylene.

The effects of varied MMOB concentration on the hydroxylase and oxidase activities of the sMMO could not be

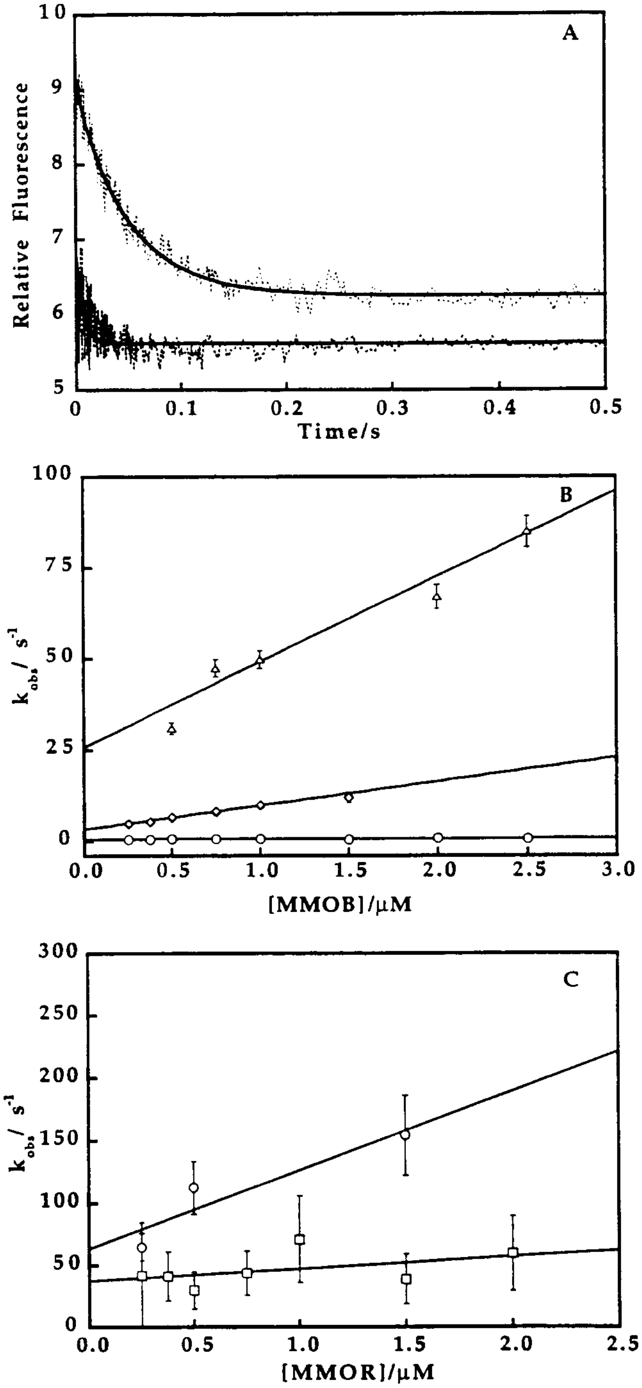

FIGURE 7: Kinetics of protein complex formation: (A) Single-exponential fits through data recording the quenching of tryptophan fluorescence associated with MMOH/MMOB (upper trace) and MMOH/MMOR (lower trace) complex formation. (B) Best linear fits through plots of observed rate constants of MMOH/MMOB complex formation at (○) 4 °C, (◇) 25 °C, and (△) 45 °C. (C) Best linear fits through plots of observed rate constants of MMOH/MMOR complex formation at (□) 25 °C and (○) 45 °C. MMOH concentration was 50 nM in all reactions.

fit with the competitive model, even when the K_d values associated with MMOR binding were decreased into the nanomolar range (Figure 5A). The competitive sites model (Scheme 1A) predicts an increase in MMOR-based oxidase activity as increasing concentrations of MMOB displace MMOR from binding sites on the hydroxylase, which does not agree with the data. The noncompetitive sites model, on the other hand, provides an excellent fit through the data and correctly predicts the MMOB concentration-dependent interconversion of MMOH oxidase and hydroxylase activities (Figure 5B).

In fitting the steady-state kinetic data, calorimetrically determined binding constants were used as initial estimates for protein−protein dissociation constants (Figure 5B). These values provided quite a good fit to steady-state data from reactions that included reductase concentrations less than that of the hydroxylase. As MMOR concentrations were increased to match or exceed the concentration of MMOH, however, the apparent concentrations of MMOB necessary to activate and inhibit the hydroxylase also increased. In the fits shown in Figure 5C,D, K_d values for MMOR binding were fixed at calorimetric estimates of 0.6 and 1.1 μM, respectively. The K_d values for MMOB binding were increased from 1.3 and 1.5 μM at 1 μM MMOR to 1.9 and 2.2 μM at 4 μM MMOR (see eqs 6 and 7). Least-squares fits through these data resulted in a consistent set of rate parameters: $k_{cat}(R_{oxidase}) = 0.33 \pm 0.12\ s^{-1}$; $k_{cat}(HR_{oxidase}) = 0.55 \pm 0.10\ s^{-1}$; $k_{cat}(HBR_{hydroxylase}) = 1.96 \pm 0.45\ s^{-1}$; and $k_{cat}(HB_2R_{hydroxylase}) = 0.32 \pm 0.18\ s^{-1}$.

The data given in Figure 6 show that propylene reacts more efficiently with sMMO at high MMOR concentration than does methane. Propylene oxidation and NADH consumption remain tightly coupled over the entire range of MMOR concentrations investigated. NADH and methane oxidation are tightly coupled only when MMOR is present in an amount less than or equal to about 20% of the hydroxylase concentration. As the MMOR concentration is raised above this limit, significantly more than one molecule of NADH is consumed for each molecule of methane oxidized. Possible implications of this finding are discussed below.

Kinetics of Complex Formation. Complex formation between MMOH and MMOR or MMOB results in a decrease in intrinsic tryptophan fluorescence. It was therefore possible to monitor the kinetics of complex formation by stopped-flow fluorescence spectroscopy. Under pseudo-first-order conditions with MMOR or MMOB present in excess, the MMOH binding kinetics are characterized by a single-exponential decrease in sample fluorescence (Figure 7A). Following this initial reaction, additional fluorescence changes occur with half-times in the seconds to tens-of-seconds range (data not shown). Some of these changes may contain information about slower structural rearrangements that are triggered by the initial binding step. They are complicated by photochemical bleaching of intrinsic MMOB fluorescence, however, and by increases in MMOH fluorescence, which also occur on this time scale. Plots of the first observed rate constant as a function of MMOB concentration are depicted in Figure 7B. The linearity of these plots supports a kinetic model in which the first observed rate corresponds to the initial MMOH/MMOB association step. In the context of the noncompeting, interacting sites model discussed above, this result implies that the structural isomerization, which communicates the binding of the first molecule of MMOB to the second MMOB binding site, is slow compared with the dissociation rate for MMOB from the precomplex (Scheme 3). On this basis, we conclude that the K_d value calculated from the ratio of the association and dissociation rate constants pertains to the MMOH/MMOB precomplex, whereas that measured by isothermal titration calorimetry is the product of K_d and the reciprocal of the subsequent

Table 3: Kinetics Rate Constants for Component Binding[a]

rate constant	MMOH + MMOB			MMOH + MMOR	
	45 °C	25 °C	4 °C	45 °C	25 °C
k_1 ($M^{-1}\ s^{-1}$)	$(2.35 \pm 0.35) \times 10^7$	$(6.6 \pm 0.1) \times 10^6$	$(8.6 \pm 1.3) \times 10^4$	$(6.3 \pm 1) \times 10^7$	$(1.0 \pm 0.15) \times 10^7$
k_{-1} (s^{-1})	25.6 ± 3.8	3.2 ± 0.5	0.56 ± 0.08	63 ± 9	38 ± 6
k_2 (s^{-1})	0.256	0.032	0.0056	0.63	0.38
k_{-2} (s^{-1})	0.0116	0.0123	0.00079	0.40	0.057

[a] Rate constants correspond to the mechanism given in Scheme 3. Association and dissociation rate constants were calculated from the slope and intercept of plots given in Figure 7.

Scheme 3

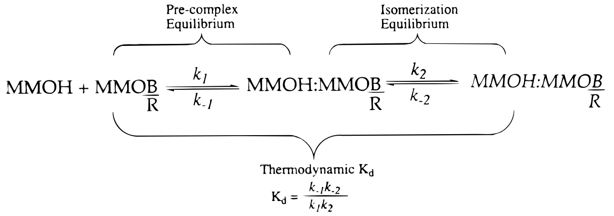

Scheme 4

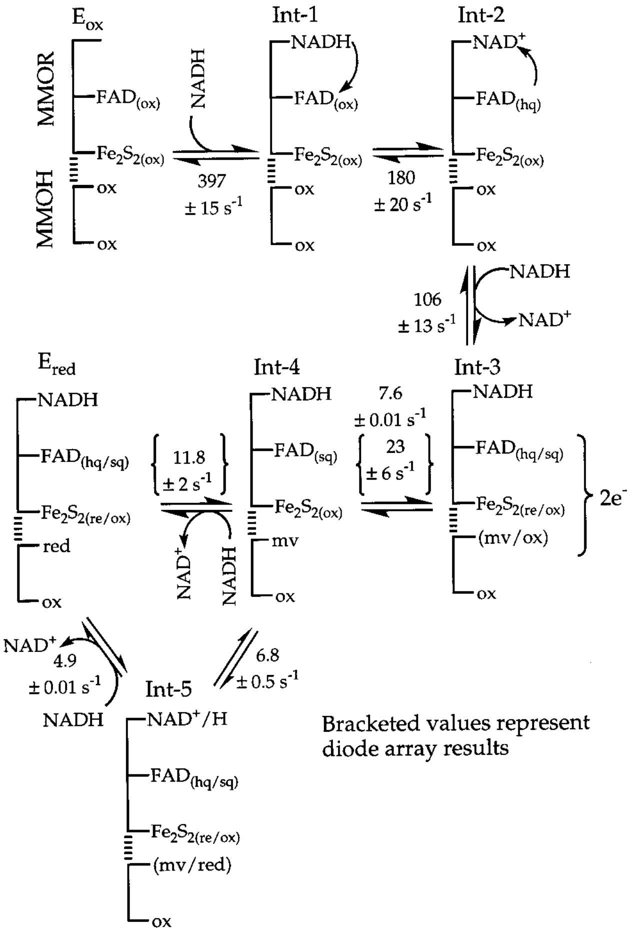

Bracketed values represent diode array results

isomerization equilibrium constant. Estimates of rate constants for the isomerization reaction, consistent with the observed kinetic resolution of the binding and isomerization reactions, are given in Table 3. These calculations were based on the assumption that a forward isomerization rate constant 2 orders of magnitude smaller than the MMOB dissociation rate constant will render the isomerization kinetics transparent in the binding phase of the reaction. The present data do not provide information about the kinetics of binding at the second MMOB and MMOR binding sites on the hydroxylase.

Table 4: Millimolar Extinction Coefficients of Intermediate States

	MMOH/MMOR complex						
	E_{ox}	Int-1	Int-2	Int-3	Int-4	Int-5	E_{red}
ϵ_{625} ($mM^{-1}\ cm^{-1}$)	1.5	3.0	2.3	2.4	3.8	3.4	2.3
ϵ_{458} ($mM^{-1}\ cm^{-1}$)	20.8	18.2	13.2	9.4	11.2	8.8	5.7

	MMOR alone			
	Ox	CT-1	CT*	SQ
ϵ_{725} ($mM^{-1}\ cm^{-1}$)	0.9	2.4	3.0	1.0
ϵ_{625} ($mM^{-1}\ cm^{-1}$)	1.5	2.7	2.7	3.5
ϵ_{458} ($mM^{-1}\ cm^{-1}$)	20.8	17.7	11.9	7.3

The fluorescence changes associated with complex formation between MMOH and MMOR are very small (Figure 7A), so the calculated estimates of association and dissociation rate contants are only approximate. Without further evidence, we suggest that MMOR, like MMOB, may bind to the hydroxylase in a two-step process characterized by precomplex formation followed by site isomerization. By using the thermodynamically and kinetically derived binding equilibrium constants, approximate values for the isomerization equilibrium and rate constants were calculated for the MMOR binding reaction (Table 3).

Electron-Transfer Reactions Leading to MMOH Reduction. The pre-steady-state reactions of NADH and MMOR were monitored by single- and multiple-wavelength stopped-flow absorbance spectroscopy. Optical transitions occurring in the reaction of MMOR with NADH at 458, 625, and 725 nm are shown in Figure 8A. Data at 725 nm report the formation and decay of pyridine nucleotide−flavin charge-transfer complexes (*39*). The initial absorbance increase ($\Delta\epsilon = 1.5\ mM^{-1}\ cm^{-1}$) at this wavelength ($k_{app} = 397\ s^{-1}$) corresponds to formation of a complex characterized by a charge-transfer band between bound NADH and the oxidized FAD moiety (Int-1 in Scheme 4). Subsequently, NADH transfers hydride to the FAD ($k_{app} = 180\ s^{-1}$), resulting in a secondary charge-transfer band ($\epsilon_{725} = 3.0\ mM^{-1}\ cm^{-1}$) between $FADH^-$ and NAD^+. This complex decomposes with $k_{app} = 106\ s^{-1}$ as NAD^+ is released from the two-electron-reduced enzyme. At 625 nm, the development of the flavin and pyridine nucleotide charge-transfer bands is followed by a further increase in absorbance associated with the formation of a neutral FAD semiquinone ($\epsilon_{625} = 3.5\ mM^{-1}\ cm^{-1}$). Semiquinone accumulates as a result of intramolecular electron transfer from the $FADH^-$ to the [2Fe-2S] center of MMOR. This reaction occurs at the NAD^+ release rate and may be coupled to pyridine nucleotide dissociation. At 458 nm, absorbance decreases are observed with k_{app} values of 180 and 106 s^{-1}. These changes are primarily due to reduction of FAD by hydride transfer ($\Delta\epsilon = 7.6\ mM^{-1}\ cm^{-1}$) followed by partial [2Fe-2S] reduction by intramolecular electron transfer ($\Delta\epsilon = 3.8\ mM^{-1}\ cm^{-1}$) (see Scheme 4 and Table 4).

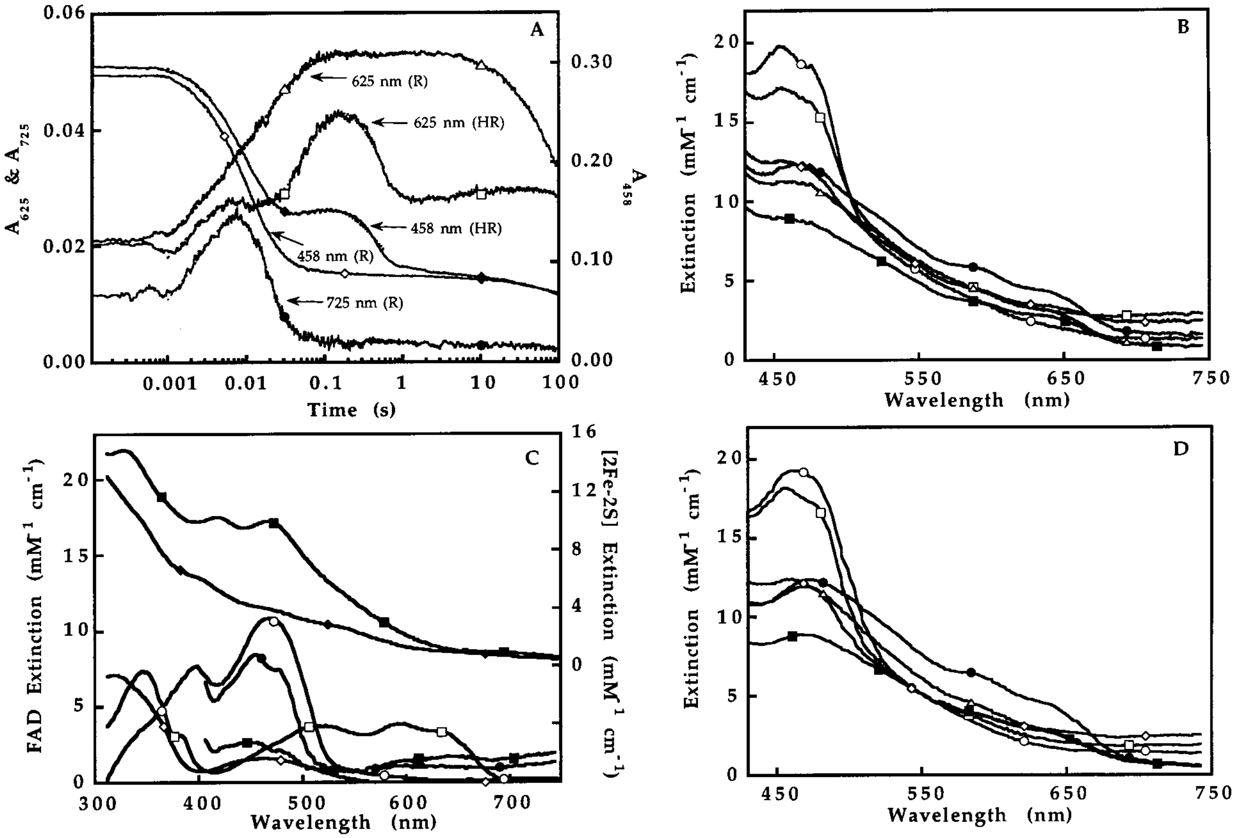

FIGURE 8: Intra- and intermolecular electron-transfer reactions in the sMMO system at 4 °C. (A) Kinetic traces recording the reaction of 15 μM MMOR with 100 μM NADH at (◇) 458 nm, (△) 625 nm, and (●) 725 nm. These data traces are compared with traces at (◆) 458 nm and (□) 625 nm from corresponding reactions in which 15 μM MMOH was present. Sequential exponential fits (···) are superimposed on the data. (B) Intermediate spectra from global analysis of multiwavelength diode array data recording the reaction of 15 μM MMOR and 15 μM MMOH with 100 μM NADH: (○) E_{ox}, (□) Int-1, (◇) Int-2, (△) Int-3, (●) Int-4, (■) E_{red}. Intermediate structures corresponding to these spectra are depicted in Scheme 4. (C) MMOR component spectra: FAD (○) oxidized, (●) CT-1, (■) CT*, (□) semiquinone, (◇) hydroquinone, and ferredoxin (■) oxidized and (◆) reduced spectra. (D) Summations of MMOR component spectra corresponding to the compositions of the intermediate structures shown in Scheme 4. In these calculations, the mixed redox states of the FAD and iron−sulfur centers of Int-3 and E_{red} were estimated by assuming equal populations of oxidized and reduced states of iron−sulfur and FAD components. Symbols delineating these spectra are the same as those used in Figure 8B.

Time-resolved single-wavelength optical data from the reaction of a 1:1 complex of MMOR and MMOH with NADH are superimposed on data from the reaction of MMOR alone with NADH in Figure 8. The compositions of intermediates proposed to accumulate during this reaction, shown in Scheme 4, are supported by comparison of the spectra calculated by global analysis of diode array data recording the reaction (Figure 8B and Table 4) with appropriate linear combinations of the component spectra (Figure 8D).

The data at 625 and 725 nm corresponding to pyridine nucleotide charge-transfer complexes of MMOR are not influenced by bound hydroxylase. Less semiquinone accumulates, however, in the reaction of the MMOH/MMOR complex with NADH (compare traces at 625 nm in Figure 8 between 10 and 100 ms), and reduction of the ferredoxin center of MMOR (detected as an absorbance decrease at 458 nm between 0.1 and 1 s) is significantly delayed in the reaction of the complex with NADH. We conclude that after the iron−sulfur center of MMOR is reduced by intramolecular electron transfer, it is rapidly reoxidized by intermolecular electron transfer to the diiron center of MMOH to form mixed-valent hydroxylase. This process is observed in two reaction steps. In the first stage of the intermolecular electron transfer reaction, MMOH is partly reduced as Int-2 converts to Int-3 (Scheme 4). The intermolecular electron transfer goes to completion in a second, slower step, resulting in an intermediate with the spectral characteristics of oxidized ferredoxin and FAD semiquinone (transition from Int-3 to Int-4 in Scheme 4). It is possible that the second phase of this reaction may be delayed due to a coupled protein conformational change. Subsequently, electron transfer from the neutral FAD semiquinone through the ferredoxin center of MMOR results in reduced hydroxylase (transition from Int-4 to E_{red} in Scheme 4). The oxidized FAD moiety generated in this step does not accumulate since it is reduced rapidly by hydride transfer from bound NADH. The product of these reduction steps is thus proposed to have four electrons distributed between the FAD and iron−sulfur centers of the reductase and one of the hydroxylase iron centers, as represented by E_{red} in Scheme 4.

In the transition from Int-3 to Int-4 (Scheme 4), intra- and intermolecular electron transfer reactions result in the accumulation of mixed-valent hydroxylase, oxidized ferredoxin, and flavin semiquinone (see 625 nm data in Figure 8A recorded between 20 and 100 ms). Diode-array analysis reveals these transitions to take place with a net rate constant of 23 s^{-1}. This value is significantly larger than that calculated for the same transition from single-wavelength data (7.6 s^{-1}). Subsequently, the mixed-valent hydroxylase

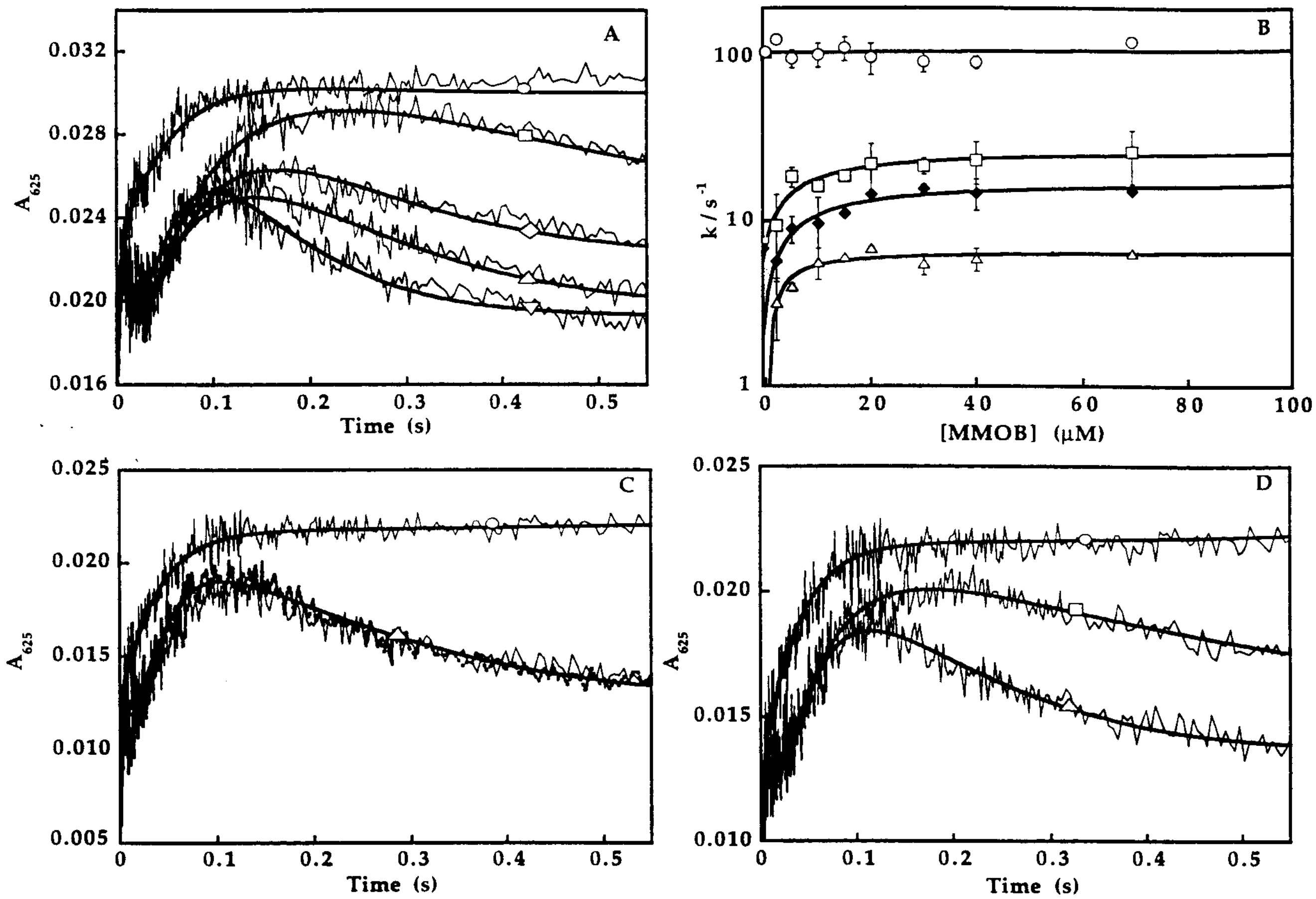

FIGURE 9: Dependence of electron-transfer kinetics on MMOB, CH_4, and CH_3OH concentration. (A) Reaction of 10 μM MMOR with 200 μM NADH and 10 μM MMOH in the presence of various concentrations of MMOB. Data records are shown for reactions that included (○) MMOR alone, (□) the MMOH/MMOR complex, and the MMOH/MMOR complex reacting with (◇) 10 μM MMOB, (△) 20 μM MMOB, and (▽) 40 μM MMOB. (B) Linear and hyperbolic fits through observed rate constants. At saturating MMOB concentrations, the observed rate constants approach values of (○) $k_3 = 106$ s^{-1}, (□) $k_4 = 27.5$ s^{-1}, (◆) $k_5 = 17.8$ s^{-1}, and (△) $k_6 = 6.5$ s^{-1}. (C) Kinetic trace recording the reaction of (○) 12 μM MMOR with 200 μM NADH, is compared with traces from reactions that also included (△) 12 μM MMOH and 5 equiv of MMOB in the (···) presence or (—) absence of saturating methane. (D) Reaction of (○) 12 μM MMOR with 200 μM NADH compared with traces from reactions that included equimolar MMOH and 5 equiv of MMOB in the (□) presence or (△) absence of 1 M methanol.

is reduced by intermolecular electron-transfer, and MMOR reacts further with NADH, resulting in partly reduced MMOR and MMOH (E_{red} in Scheme 4). These last two electron-transfer steps were best fit as a single kinetic phase with a rate constant of 11 s^{-1} from the diode-array data. As discussed below, two exponentials were required to provide good fits to single-wavelength data recorded in this time domain. The differences between the diode-array and single-wavelength results probably arise from photochemistry induced by the 75 W xenon lamp in the former study since, as mentioned above, we observe photochemical reactions on this time scale in stopped-flow fluorescence experiments with the same light source.

Extinction coefficients for the intermediate species calculated from single-wavelength fits (Table 4) are consistent with the transitions described above. Since the reactions monitored by diode-array detection are influenced by photochemistry, and reversibility was not considered in the data analysis, the intermediate spectra presented in Figure 8B should be treated only as approximations, and the main information afforded by this analysis pertains to the reaction sequence.

Effects of MMOB, Methane, and Methanol on the Rate of Intermolecular Electron Transfer from MMOR to MMOH. The dependence of the intermolecular electron-transfer reactions from MMOR to MMOH on added MMOB, substrate, and product was investigated by stopped-flow spectroscopy. Data recorded at 625 nm reveal that the intermolecular electron-transfer reaction depends on MMOB concentration (Figure 9A). These data were fit after fixing rate constants for NADH binding and hydride transfer to values calculated for the corresponding reactions in the reductive half-reaction involving only MMOR (Scheme 4). Four rate constants were then allowed to vary in the fitting procedure. A plot of the best-fit observed rate constants as a function of MMOB concentration is given in Figure 9B. The first rate constant is independent of MMOB concentration and corresponds to the first intermolecular electron-transfer step from MMOR to MMOH (106 ± 13 s^{-1}). The reaction appears to occur as rapidly as the ferredoxin center of MMOR is reduced by intramolecular electron transfer. This rate constant is independent of MMOB concentration since the electron delivery rate to the hydroxylase cannot exceed the rate of intramolecular electron transfer from the FAD to the ferredoxin center of the reductase. The remaining three rate constants corresponding to intermolecular electron transfers from MMOR to MMOH all increase with MMOB concentration.

Table 5: Intermolecular Electron-Transfer Rates[a]

ET complex	k_4 (s^{-1})	k_5 (s^{-1})	k_6 (s^{-1})
MMOH + 1 equiv of MMOR	7.6 ± 0.01	6.8 ± 0.5	4.9 ± 0.01
MMOH + 1 equiv of MMOR + 5 equiv MMOB	24.5 ± 0.6	15.8 ± 1.5	6.4 ± 0.1
MMOH + 1 equiv of MMOR + 5 equiv MMOB + 0.5 mM CH_4	24.5 ± 1.5	21.7 ± 2.2	6.0 ± 1.7
MMOH + 1 equiv of MMOR + 5 equiv MMOB + 1 MCH_3OH	11.2 ± 0.1	11.0 ± 0.1	1.2 ± 0.4

[a] Rate constants correspond to kinetic transitions involved in the conversion of Int-3 to E_{red} through Int-5 as shown in the last three steps in Scheme 4.

Figure 9C illustrates the effect of including saturating amounts of methane in the reaction of the MMOH/MMOR complex with NADH. The superimposability of the traces makes it clear that, even at saturating concentrations, methane has no significant effect on the electron transfer kinetics. The effect of including 1 M methanol in the reaction is illustrated in Figure 9D. At this concentration, a significant fraction of methanol should be bound at the diiron(III) active site of MMOH (*40*). These data suggest that the first, MMOB concentration-independent, electron-transfer rate is not affected by methanol; however, the subsequent MMOB concentration-dependent steps are significantly retarded. Rate constants from exponential fits of these data are given in Table 5.

DISCUSSION

The soluble methane monooxygenase system orchestrates a series of electron-transfer and substrate-activation reactions that enable the catalytic conversion of methane and dioxygen gases to methanol and water. The success of this chemistry depends on the ability of sMMO to generate a highly reactive intermediate capable of inserting an oxygen atom into a C−H bond of methane without damaging the active site of the hydroxylase. Dynamic interactions between the reductase, hydroxylase, and regulatory proteins ensure both efficiency and sustainability of the hydroxylation reaction.

Regulation and Switching of sMMO Hydroxylase, Oxidase, and Peroxidase Activities. The sMMO system has the diverse catalytic ability to function as a hydroxylase, oxidase, or peroxidase. The interchangeability of these activities depends on both the availability of appropriate substrates and the relative concentrations of MMOH, MMOR, and MMOB present in reaction mixtures.

We find that the sMMO system operates most efficiently as a hydroxylase when the concentration of MMOR is about $^1/_5$ that of MMOH and when the MMOB concentration is greater than or equal to that of the hydroxylase. Under these conditions, methane hydroxylation and NADH consumption occur with approximately 1:1 stoichiometry. The rate of substrate hydroxylation further increases at higher MMOR concentrations, but with decreased catalytic efficiency, such that more than one mole of NADH is consumed for each mole of methane oxidized. Increasing the MMOB concentration at fixed MMOR concentration decreases the rate of the hydroxylation reaction without uncoupling methane and NADH consumption. The sensitivity of the hydroxylation reaction to MMOB and MMOR concentrations is apparent at temperatures from 4 to 45 °C, suggesting that the regulatory mechanism of the hydroxylation is conserved over this temperature range.

In the absence of hydrocarbon substrates, the sMMO system continues to consume NADH and dioxygen in an oxidase reaction, which is catalytic for hundreds of turnovers and does not release hydrogen peroxide or other reactive oxygen species into solution. Our data support the previous conclusion that the oxidase activity involves the four-electron reduction of dioxygen to water (*11*). This idling mode of the hydroxylase may serve to protect the potentially susceptible amino acids in the active site from oxidative damage that otherwise might occur when substrate is unavailable. When substrate is added, the hydroxylase activity of the sMMO system is immediately restored. It therefore appears that binding of hydrocarbon substrate serves as a molecular switch that converts sMMO from an oxidase to a hydroxylase. When MMOB is excluded from the reaction, MMOH and MMOR form a complex that catalyzes a second type of oxidase reaction. This reaction is distinguished from the idling state described above because it continues independent of the availability of hydrocarbon substrate. The oxidase activity of the MMOH/MMOR complex can be diverted to hydroxylase activity by addition of MMOB. Thus, oxidase activity resulting in the reduction of molecular oxygen to water at the active site of MMOH can be diverted to hydroxylase activity through the introduction of either MMOB or a small organic substrate. Our findings are in disagreement with a previous report, which suggested that, in the absence of substrate, oxidase activity was inhibited by the addition of MMOB (*11*).

As MMOR concentrations are increased to match and exceed that of the hydroxylase in reactions with methane, the system becomes uncoupled, consuming more NADH than required for efficient substrate hydroxylation. We show that MMOR can deliver electrons to the hydroxylase with a rate constant that is 1−2 orders of magnitude greater than the conversion rate of H_{peroxo} to Q (*41*). Moreover, the reductase can rapidly bind and dissociate from the hydroxylase, enabling a small population of MMOR molecules to service a much greater population of MMOH molecules. We therefore propose that this third kind of oxidase activity is due to the reduction of peroxo and Q intermediates of the MMOH reaction cycle at a rate that competes with the substrate hydroxylation reaction. The oxidase reaction occurs to a much lesser extent when propylene is substituted for methane because propylene can react directly with H_{peroxo}, whereas methane hydroxylation requires formation of intermediate Q (*41*). Studies of the steroyl-acyl carrier protein Δ^9-desaturase, which indicate that the peroxydiiron(III) intermediate of this enzyme can be induced to release water if provided with a source of electrons (*42*), provide additional support for this hypothesis. It was proposed on the basis of the results of single-turnover reactions of the sMMO (OB3b) system that MMOB may prevent the reduction of oxygen intermediates in this system (*14*). Our data, on the other hand, indicate that saturating MMOH with MMOB actually increase the rate of electron transfer from MMOR to the diiron active sites of the hydroxylase. Moreover, when MMOR concentrations are elevated, the rate at which active oxygen intermediates are reduced to water competes with the rate of substrate hydroxylation.

Free MMOR reacts slowly with NADH and dioxygen in a hydrogen peroxide-generating oxidase reaction. Since the sMMO (Bath) system as isolated contains a relatively low concentrations of MMOR and significant concentrations of MMOB (*5*), we conclude that the most physiologically relevant oxidase activity is that switched on and off in response to changes in methane concentration.

We show here that the complete sMMO system reacts rapidly as an NADH peroxidase at micromolar concentrations of hydrogen peroxide. This reaction, which occurs in the presence or absence of MMOB and substrate, consumes equimolar amounts of hydrogen peroxide and NADH. It is possible that the added hydrogen peroxide binds directly to the diiron(III) active site of the hydroxylase where it is reduced by two NADH-derived electrons to water. Alternatively (Scheme 2A), hydrogen peroxide may compete with dioxygen and react with the diiron(II) center of the hydroxylase. Finally, the added hydrogen peroxide may donate two electrons to a reactive oxygen intermediate such as H_{peroxo}. These possibilities are difficult to distinguish from each other since all three reactions consume hydrogen peroxide and result in no net change in oxygen concentration. The first mechanism is disfavored since it was previously shown that hydrogen peroxide binds too weakly and reacts too slowly with H_{ox} to account for the peroxidase activity (*12*, *43*). The second mechanism requires that hydrogen peroxide can effectively compete with molecular oxygen for diiron(II) sites of MMOH. The third mechanism requires only that hydrogen peroxide enter the sMMO active site and react with a preexisting oxygen intermediate, H_{peroxo}. The NADH peroxidase activity of sMMO may be a physiologically relevant means of depleting the cytosol of potentially toxic levels of hydrogen peroxide during the growth of *M. capsulatus* (Bath). The mechanisms of the peroxidase and oxidase reactions are areas of present investigation as will be reported in detail at a later time.

Stoichiometry and Stability of Complexes Formed by the sMMO System. The X-ray crystal structure reveals that MMOH is a dimer of equivalent protomers. The equilibrium analytical ultracentrifugation data presented here indicate that MMOB and MMOR exist as monomers in solution. Additional support for the monomeric nature of MMOB comes from studies of a series of truncated MMOB mutants (*20*). This work suggests that MMOB is a monomer but that it migrates anomalously in gel-filtration chromatographic separations due to the structural properties of its N-terminus (*20*). Moreover, we observe no changes in fluorescence intensity or binding enthalpy to signal the formation of complexes of MMOB with MMOR. This observation is in contrast with data from the sMMO (OB3b) system, where it has been reported that MMOB and MMOR form a high-affinity complex (*26*). Given the known similarities of the sMMO proteins from these systems, it is surprising that such a difference could exist.

After submission of this paper, low-angle X-ray scattering studies were reported that address the nature of complexes formed between MMOH and the other protein components of sMMO (Bath) (*44*). In agreement with our ITC data, these X-ray studies are most consistent with protein complex stoichiometries of 2:1 for each MMOB and MMOR binding to MMOH (*44*). In addition, this work proposed a major change in the structure of MMOH in complexes with (MMOB = MMOR):MMOH ratios ≥ 10, far above the values that we find here can account for the equilibrium binding and other data. Fits through our calorimetric data from titrations of the MMOH/MMOR complex with MMOB indicate no significant decrease in MMOB binding affinity or stoichiometry. On this basis we conclude that MMOB and MMOR bind at distinct sites on the hydroxylase and do not exclude each other from binding. Given these results, we propose that ternary complexes of hydroxylase, regulatory protein, and reductase may form during catalysis with a maximum complex stoichiometry of 2 MMOB, 2 MMOR, and 1 MMOH.

Evidence for Regulation through Noncompetitive Binding. The conversion of sMMO (Bath) from an oxidase to a hydroxylase, and the activation and inhibition of the substrate hydroxylation reaction, are regulated by changing the concentration of MMOB. We have explored competitive and noncompetitive binding mechanisms that account for these functions of the regulatory protein. The competitive mechanism is similar to that used to model steady-state data from the sMMO (OB3b) system (*26*). Our analysis differs principally from that previously reported for the sMMO (OB3b) system in that we simultaneously fit data sets corresponding to both the oxidase and hydroxylase activities of sMMO (Bath) and judge these fits on the basis of their agreement with data corresponding to each type of activity. Only the hydroxylase activity was reported and considered in the previous fits (*26*), so it is not possible to judge how well the oxidase component of the sMMO (OB3b) activity agrees with predictions of the competitive model. Our fitting results for the sMMO (Bath) system lead us to favor a noncompetitive model of component interactions.

A major feature distinguishing the competitive and noncompetitive models is their ability to fit simultaneously the oxidase and hydroxylase activities of the sMMO system in the presence of saturating amounts of MMOB. The noncompetitive model correctly predicts both that the sMMO system remains coupled with respect to NADH consumption and substrate hydroxylation in the presence of saturating MMOB and that a nonzero rate of inhibited catalysis is asymptotically approached under these conditions. In contrast, the competitive model predicts that the hydroxylase activity will drop to near zero as MMOB displaces MMOR and that free MMOR will catalyze oxidase activity, resulting in an uncoupled state.

Additional support for the existence of distinct noncompetitive MMOR and MMOB binding sites comes from the intermolecular electron-transfer studies presented here. The data from these studies reveal that MMOB has an important role in accelerating intermolecular electron transfer from MMOR to MMOH such that the rate increases to a limiting value as the hydroxylase becomes saturated with MMOB. From our fluorescence measurements we estimate the rate constant for dissociation of MMOB from the hydroxylase at 4 °C to be 0.56 s^{-1}. This value is much smaller than the largest observed rate constant (106 s^{-1}) for intermolecular electron transfer from MMOR to MMOH. Thus, MMOB and MMOR cannot be competing for binding sites, since it would not be possible for MMOB to dissociate from the hydroxylase fast enough for MMOR to bind and deliver electrons to MMOH at the observed rate constant of intermolecular electron transfer.

Location of MMOR and MMOB Binding Sites on the Hydroxylase. Both interacting and noninteracting site models are possible in systems that bind multiple ligands. In the case of sMMO, however, the investigated complexes are macromolecular and involve large surface areas. It is therefore improbable that binding at one site on the hydroxylase surface would not have at least a subtle effect on the remaining unoccupied binding site. The C_2 axis relating the hydroxylase protomers (*31*) implies that MMOR and MMOB must each have two symmetry-related binding sites (Scheme 1B) unless these sites are located at the poles of MMOH, as illustrated in Scheme 1C. The diiron centers of the hydroxylase are located just beneath the floor of canyons formed by the protomers of MMOH and thus quite far from distal binding sites at the poles of the enzyme (*31*). Binding in the canyon region would position the ferredoxin domain of the reductase near the dinuclear iron center in the hydroxylase α-subunit, poising the system for efficient intermolecular electron transfer. Binding of MMOB in the canyon region would similarly position it in close proximity to the diiron center of the hydroxylase. We conclude solely on the basis of these structural arguments that MMOB and MMOR are both likely to bind at interacting sites in the canyon regions that are related by the symmetry axis of the hydroxylase.

Our data that reveal tryptophan fluorescence quenching when either MMOB or MMOR binds to the hydroxylase are consistent with the proposed location of MMOB and MMOR binding sites, since multiple tryptophan residues are present in the canyon (*45*). Tryptophan fluorescence quenching similarly was reported in titrations of MMOH (OB3b) with MMOR from that system (*26*). Finally, chemical cross-linking data from the sMMO (OB3b) system imply that MMOB interacts closely with the α-subunit and MMOR with the *β*-subunit of MMOH (OB3b) (*26*). Additional interactions of the reductase with the α-subunits of the hydroxylase have been suggested on the basis of modeling studies (*46*).

Interpretation of Thermodynamic and Kinetic Binding Data. The binding of MMOB to each of its two sites on MMOH is endothermic and entropy-driven at temperatures below 30 °C. At higher temperatures, these reactions become exothermic, and at 45 °C enthalpy and entropy make similar contributions to the free energy of binding. The temperature dependence of the enthalpy of binding implies that a conformational change may occur as a function of temperature that affects the MMOH/MMOB binding interface (*47*). Interestingly, the temperature-dependent enthalpy change is paralleled by a compensatory change in entropy that serves to dampen the increase in binding free energy with temperature. Our studies of the temperature dependence of the MMOB-dependent activation and inhibition of hydroxylase activity and interconversion of oxidase and hydroxylase activities disfavor a global change of mechanism linked to the conformational change. Details of the high- and low-temperature conformations of the MMOH/MMOB complexes are presently unknown and await elucidation by advanced structural analysis.

The MMOR binding reactions are also entropy-driven, but the enthalpy of MMOR binding to the hydroxylase is essentially temperature-independent. This result distinguishes the MMOB and MMOR binding sites and suggests that the observed temperature-dependent conformational change is not global and may be limited to specific contacts at the MMOH/MMOB binding interface. The entropy changes that drive the MMOR and MMOB binding reactions probably derive in part from the increase in disorder associated with the displacement of water molecules from the MMOR and MMOB binding interfaces of the hydroxylase (*48*).

In our initial fits of the calorimetry data, we found that the number of binding sites was typically 60−80% of the value predicted from the hydroxylase concentration calculated from its extinction coefficient at 280 nm. To correct for this apparent noninteger site occupancy, the hydroxylase concentration value used in the final data fitting was decreased by 20−40% from the value calculated by using the extinction coefficient of MMOH at 280 nm. The apparent values of the dissociation constants changed by 10−20% as a result of this correction. The uncertainty in hydroxylase extinction coefficient, calculated from the results of total amino acid analysis, is not large enough to account for this result, and it appears that about 30% of the hydroxylase is incapable of binding to reductase and regulatory protein. At present we cannot state whether these MMOB and MMOR sites are damaged or just temporarily unavailable. MMOH preparations typically contain less than a stoichiometric amount of iron, which may in part account for the nonbinding population detected in the ITC studies. The 2:1 MMOB and MMOR binding stoichiometries of the hydroxylase, calculated by fitting the ITC data, agree with those calculated from fits through the X-ray scattering data (*44*) and EPR titrations (*26*).

The temperature dependence of the enthalpy of the binding of MMOB to MMOH implies that the structure of the interface through which the hydroxylase and regulatory protein interact changes as a function of temperature. The enthalpy of the binding of MMOR to MMOH, however, is independent of temperature, which implies that structure of the binding interface of MMOR and MMOH is not greatly affected by temperature. We no evidence to support a binding interaction of the reductase and MMOB protein by ITC. We recently confirmed this result by solution NMR studies in which it was demonstrated that MMOB and MMOR do not interact significantly when free in solution or when bound at their respective sites on the surface of the hydroxylase (*49*). On this basis our results do not entirely support the interpretation of the X-ray scattering data, which suggests that a large conformational change of MMOH occurs upon binding MMOB and MMOR (*44*).

Binding Kinetics and Steady-State Catalysis. We propose a two-step kinetic model to explain protein component binding to the hydroxylase. The first stage of binding, which we have monitored by stopped-flow fluorescence spectroscopy, is characterized by MMOB or MMOR associating with the hydroxylase to form a rapidly equilibrating precomplex. These precomplexes more slowly isomerize to afford the thermodynamically stabilized equilibrium complexes that we detect by ITC. Thus, the equilibrium constants calculated from ITC data are the product of a binding constant and an isomerization equilibrium constant. The isomerization component of the thermodynamic equilibrium corresponds to a structural change, which transmits information about component binding to unoccupied sites and is responsible for the observed negative cooperativity between sites. Our best estimates for isomerization rate constants suggest that MMOB and MMOR can bind and dissociate rapidly from precomplexes with MMOH and that the precomplexes isomerize to form equilibrium complexes much more slowly. Thus, MMOR can bind and dissociate rapidly from a large population of oxidized MMOH. This observation and the rapid (100 s^{-1}) electron-transfer rate constant are consistent with our steady-state kinetic data, which show that a small population of MMOR is able to react with a significantly larger population of MMOH during turnover. During catalysis MMOB and MMOR interact not only with oxidized but also with reduced and substrate- and product-bound states of the hydroxylase. The significance of these interactions is considered below.

Oxidation−reduction and protein component binding equilibria of the hydroxylase are linked such that MMOB binding decreases (*50*, *51*) and MMOR binding increases (*14*, *52*) the hydroxylase diiron center midpoint potential. The MMOB-induced decrease in equilibrium midpoint potential is canceled in ternary complexes of MMOH, MMOB, and MMOR (*14*). Considering this linkage of ligand binding and redox equilibria, it can be concluded that reduction of MMOH/MMOB complexes by MMOR will result in the formation of tightly assembled ternary complexes, composed of MMOB, MMOR, and reduced hydroxylase. We propose that such complexes bind and react with molecular oxygen during catalysis.

Our steady-state data indicate that MMOR can transfer electrons to several hydroxylase molecules in the time it takes for MMOH to complete a single turnover. Since the reductase is tightly bound in the complex formed with reduced hydroxylase and MMOB (*14*), its binding affinity must dramatically decrease during the reaction of MMOH with dioxygen so that it can dissociate and react with other hydroxylase molecules. The exact point in the oxygen reaction at which this change in affinity occurs remains to be established, however. It was proposed on the basis of the results of modeling studies of the reaction of dioxygen with the MMOH/MMOB complex from sMMO (OB3b) that the binding of molecular oxygen at the diiron center results in a significant decrease in MMOB binding affinity (*13*). Additional fluctuations in the binding affinity of MMOB are proposed to occur as the peroxo and Q intermediates evolve (*13*).

Redox and protein binding equilibria of the sMMO system may be linked to changes in hydroxylase structure that regulate substrate binding and product dissociation reactions. Comparison of the high-resolution structure of oxidized MMOH with structures solved by use of data from either chemically reduced crystals or crystals grown in the presence of MMOB revealed that leucine-110 moves to assume conformations that alternately block or augment the accessibility of the diiron center (*46*). Mechanistic studies of the analogous side chain of leucine-103 in myohemerytherin identified it as having an important role in regulating the accessibility of the active site to dioxygen (*53*, *54*). Similarly, reduction of MMOH may be coupled to a movement of leucine-110, which opens a channel for the entry of molecular oxygen to access the diiron center (*46*).

Delivery of Electrons to the Active Site of MMOH. Methane monoxygenase employs a sophisticated electron delivery system that is closely related to those found in a variety of related enzymes ranging from bacterial monooxygenases (*55*), dioxygenases (*39*), and photosynthetic (*56*) and respiratory (*57*) electron-transport chains.

The sMMO reductase functions by converting hydride from NADH into single-electron equivalents and then injecting them sequentially into the diiron active centers of the hydroxylase. Detailed kinetic studies of two iron−sulfur flavoenzymes that are close relatives of MMOR were recently reported (*39*, *58*). We use a combination of single- and multiple-wavelength stopped-flow data here to identify intermediate species involved in the reduction of MMOR and in the intermolecular electron transfer from MMOR to MMOH.

In the reduction reaction, NADH initially binds and forms a charge-transfer complex with the oxidized FAD moiety. Subsequently, it transfers a hydride and forms a reduced FAD and NAD^+ charge-transfer complex. Absorbance due to the charge-transfer band is then lost as NAD^+ is released from the enzyme. In the same kinetic phase, intramolecular electron transfer occurs, resulting in the formation of a FAD semiquinone and reduced [2Fe-2S] state of the reductase. The [2Fe-2S] center serves as the interface for electron transfer from MMOR to acceptor molecules, and its reduction poises MMOR for reaction with MMOH. MMOR can provide MMOH with four electrons through sequential intermolecular electron transfers from its ferredoxin domain to the oxidized dinuclear iron centers of the hydroxylase. Oxidized and fully reduced forms of the hydroxylase are optically silent in the visible region of the absorbance spectrum. Preliminary studies of single electron transfer from the ferredoxin domain of MMOR to the oxidized hydroxylase suggest that the optical changes associated with the formation of H_{mv} are small compared with those associated with redox reactions of MMOR in the visible region (*59*). Thus, to a first approximation, monitoring intermolecular electron transfer from the reductase to the hydroxylase is as simple as monitoring time-dependent optical changes associated with the oxidation of reduced MMOR.

Previous studies of electron transfer in sMMO (Bath) helped to identify optical changes associated with FAD reduction and intermolecular electron transfer from MMOR to MMOH (*11*, *16*); however, our data are inconsistent with the conclusions drawn in these papers. It was previously suggested that intramolecular electron transfer from the FAD to the [2Fe-2S] center of MMOR occurs prior to the release of NAD^+ (*16*). In our studies, however, we find that NAD^+ dissociates in the same kinetic phase in which intermolecular electron transfer from the FAD to the [2Fe-2S] occurs. It was reported that the binding of MMOB blocks intermolecular electron transfer from MMOR to MMOH and that inclusion of organic substrate in these reactions overcomes this inhibition (*16*). We find in contrast with these results that intermolecular electron transfer from MMOR to the diiron center of the hydroxylase is accelerated when MMOB is bound to MMOH and that inclusion of saturating methane has no significant effect on the electron-transfer rate.

Hydroxylation of nitrobenzene by sMMO results in the formation of a product-bound intermediate T that can be detected by its *p*-nitrophenol chromophore (*17*). The intermediate T resulting from methane hydroxylation on the other hand is colorless and cannot be detected by optical absorption spectroscopy. Single-turnover studies indicated that release of *p*-nitrophenol from the active site is rate-limiting compared with other steps in the reaction mechanism (*17*). A product-bound form of MMOH thought to be representative of intermediate T can be prepared by titrating the oxidized hydroxylase with excess methanol, and EPR studies revealed that the electronic properties of this complex are altered upon binding of MMOB (*40*). We demonstrate here that this methanol complex of the hydroxylase can be rapidly reduced by MMOR and that the inclusion of MMOB accelerates this reaction. We propose that reduction of the diiron center may decrease its affinity for coordinated methanol, serving both to facilitate product release and to prepare the diiron center for reaction with molecular oxygen.

CONCLUSIONS

The kinetics and thermodynamics of binding interactions between the oxidized components of the sMMO system were investigated by isothermal titration calorimetry and stopped-flow fluorescence spectroscopy. These studies and the results of analytical ultracentrifugation experiments indicate that at physiological concentrations MMOR and MMOB exist in solution as monomers that bind MMOH with 2:1 stoichiometry and weak negative cooperativity. Component binding occurs in a two-step process. A Michaelis complex forms initially between MMOH and MMOB or MMOH and MMOR. This step is followed by a slower isomerization reaction, which communicates the binding event to a second symmetry-related site and accounts for the negative cooperative relationship between the two sites. The temperature dependence of the thermodynamic parameters associated with complex formation suggests that the structure of the MMOH/MMOB binding interface changes as a function of temperature. Thus, MMOH and/or MMOB appear to undergo temperature-dependent conformational changes. There is no evidence that a similar temperature-dependent change occurs at the MMOR binding interfaces of the hydroxylase. It is possible that this isomerization corresponds to a structural change that is related to the greatly increased rate of catalysis by the hydroxylase at 45 °C compared with the rate at 25 °C.

Steady-state kinetic investigations of the sMMO reveal several modes of catalysis in addition to the well-studied hydroxylase activity. In the absence of MMOH, MMOR reacts with NADH and molecular oxygen to generate hydrogen peroxide. Addition of hydroxylase in the presence or absence of MMOB accelerates the rate of NADH oxidation, but the product of these reactions is water rather than hydrogen peroxide. Introduction of methane or propylene switches the oxidase activity to hydroxylase activity, but only when MMOB is present. Thus, substrate and MMOB each appear to have important roles in modulating the active-site chemistry of MMOH. Finally, the hydroxylase functions as an NADH peroxidase when supplied with electrons by MMOR in the presence or absence of MMOB and substrate. This previously overlooked activity may represent a mechanism whereby *M. capsulatus* (Bath) protects itself from the potential toxicity of hydrogen peroxide.

We have studied the catalytic efficiency of the sMMO system as defined by the extent to which NADH oxidation is coupled to substrate hydroxylation. The efficiency of the hydroxylation reaction is very sensitive to the relative component concentrations and the reactivity of the hydrocarbon substrate. The observed changes in catalytic efficiency as a function of varied MMOR and MMOB concentration allow us to rule out a mechanism in which MMOB and MMOR compete for binding sites in favor of noncompetitive binding during catalysis.

The reaction of MMOR with pyridine nucleotides affords charge-transfer and semiquinone-containing intermediates that closely resemble those observed in related iron−sulfur and flavin-containing reductases. Intermolecular electron transfer from the ferredoxin domain of MMOR to the dinuclear iron center of MMOH occurs as rapidly as electrons are delivered to the ferredoxin center by intramolecular electron transfer from FAD. Subsequent intermolecular electron-transfer reactions occur more slowly. These steps are accelerated in the presence of MMOB. Methane has no significant effect on the electron-transfer reaction. Reduction of intermediate T by intermolecular electron transfer may be an important aspect of the product release mechanism, and the reduction of the peroxo and Q intermediates may account for the uncoupled oxidase activity detected when MMOR concentrations are present in excess.

ACKNOWLEDGMENT

We thank Professor P. S. Kim for use of the isothermal titration calorimeter and analytical ultracentrifuge, D. Akey for training and helpful discussions regarding the sedimentation equilibrium technique, and J. L. Blazyk, D. A. Kopp, A. M. Valentine, and S. S. Stahl for many helpful discussions and critical reading of the manuscript.

REFERENCES

1. Higgins, I. J., Best, D. J., Hammond, R. C., and Scott, D. (1981) *Microbiol. Rev. 45*, 556−590.
2. Whittenbury, R., Phillips, K. C., and Wilkinson, J. F. (1970) *J. Gen. Microbiol. 61*, 205−218.
3. Colby, J., and Dalton, H. (1978) *Biochem. J. 171*,461−468.
4. Pilkington, S. J., and Dalton, H. (1990) *Methods Enzymol. 188*, 181−190.
5. Fox, B. G., Froland, W. A., Dege, J. E., and Lipscomb, J. D. (1989) *J. Biol. Chem. 264*, 10023−10033.
6. Fox, B. G., Froland, W. A., Jollie, D. R., and Lipscomb, J. D. (1990) *Methods Enzymol. 188*, 191−202.
7. Higgins, I. J., Best, D. J., and Hammond, R. C. (1980) *Nature 286*, 561−564.
8. Fox, B. G., Borneman, J. G., Wacket, L. P., and Lipscomb, J. D. (1990) *Biochemistry 29*, 6419−6427.
9. Feig, A. L., and Lippard, S. J. (1994) *Chem. Rev. 94*, 759−805.
10. Crabtree, R. H. (1995) *Chem. Rev. 95*, 987−1007.
11. Lund, J., Woodlund, M. P., and Dalton, H. (1985) *Eur. J. Biochem. 147*, 297−305.
12. Froland, W. A., Andersson, K. K., Lee, S.-K., Liu, Y., and Lipscomb, J. D. (1992) *J. Biol. Chem. 267*, 17588−17597.
13. Liu, Y., Nesheim, J. C., Lee, S.-K., and Lipscomb, J. D. (1995) *J. Biol. Chem. 270*, 24662−24665.
14. Liu, Y., Nescheim, J. C., Paulsen, K. E., Stankovich, M. T., and Lipscomb, J. D. (1997) *Biochemistry 36*, 5223−5233.
15. Green, J., and Dalton, H. (1986) *Biochem. J. 236*, 155−162.
16. Green, J., and Dalton, H. (1989) *Biochem. J.* 259,167−172.
17. Lee, S.-K., Nesheim, J. C., and Lipscomb, J. D. (1993) *J. Biol. Chem. 268*, 21569−21577.
18. Liu, K. E., Valentine, A. M., Wang, D., Huynh, B. H., Edmondson, D. E., Salifoglou, A., and Lippard, S. J. (1995) *J. Amer. Chem. Soc. 117*, 10174−10185.
19. Lloyd, J. S., Bhambra, A., Murrell, J. C., and Dalton, H. (1997) *Eur. J. Biochem. 248*, 72−79.
20. Brandstetter, H., Whittington, D. A., Lippard, S. J., and Frederick, C. A. (1999) *Chem. Biol. 6*, 441−449.

21. DeWitt, J. G., Rosenzweig, A. C., Salifoglou, A., Hedman, B., Lippard, S. J., and Hodgson, K. 0. (1995) *J. Am. Chem. Soc. 34*, 2505−2515.
22. Green, J., and Dalton, H. (1985) *J. Biol. Chem. 260*, 15795−15801.
23. Coufal, D. E., Blazyk, J. L., Whittington, D. A., Wu, W. W., Rosenzweig, A. C., and Lippard, S. J. (1999) manuscript in preparation.
24. Hildebrandt, A. G., and Roots, I. (1975) *Arch. Biochem. Biophys. 171*, 385−397.
25. Lakowicz, J. R. (1983) *Principles of Fluorescence Spectroscopy*, Plenum Press, New York.
26. Fox, B. G., Liu, Y., Dege, J. E., and Lipscomb, J. D. (1991) *J. Biol. Chem. 266*, 540−550.
27. Barshop, B. A., Wrenn, R. F., and Frieden, C. (1983) *Anal. Biochem. 130*, 134−145.
28. Zimmerle, C. T., and Frieden, C. (1989) *Biochem. J. 258*, 381−387.
29. Rosenzweig, A. C. (1994) Ph.D. Dissertation, p 339, Massachusetts Institute of Technology, Cambridge, MA.
30. Gill, S. C., and Hippel, P. H. (1989) *Anal. Biochem. 182*, 319−326.
31. Rosenzweig, A. C., Frederick, C. A., Lippard, S. J., and Nordlund, P. (1993) *Nature 366*, 537−543.
32. Lund, J., and Dalton, H. (1985) *Eur. J. Biochem. 147*, 291−296.
33. Shinohara, Y., Uchiyama, H., Yagi, O., and Kusakabe, I. (1998) *J. Ferment. Bioeng. 85*, 37−42.
34. Chang, S.-L., Waller, B. J., Lipscomb, J. D., and Mayo, K. H. (1999) *Biochemistry 38*, 5799−5812.
35. Cantor, C. R., and Schimmel, P. R. (1980) *Biophysical Chemistry*, Vol. 2, W. H. Freeman, San Francisco, CA.
36. Laue, T. M., Shah, B. D., Ridgeway, T. M., and Pelletier, S. L. (1992) *Analytical Ultracentrifugation in Biochemistry and Polymer Science*, Vol. 1, Royal Society of Chemistry, Cambridge, England.
37. Gennis, R. B. (1989) *Biomembranes*, Springer-Verlag, New York.
38. Wyman, J., and Gill, S. J. (1990) *Binding and Linkage*, University Science Books, Mill Valley, CA.
39. Gassner, G. T., Ludwig, M. L., Gatti, D. L., Correll, C. C., and Ballou, D. P. (1995) *FASEB J. 7*, 1411−1418.
40. Davydov, R., Valentine, A. M., Komar-Panicucci, S., Hoffman, B. M., and Lippard, S. J. (1999) *Biochemistry 38*, 4188−4197.
41. Valentine, A. M., Stahl, S. S., and Lippard, S. J. (1998) *J. Am. Chem. Soc. 121*, 3876−3887.
42. Broadwater, J. A., Ai, J., Loehr, T. M., Sanders-Loehr, J., and Fox, B. G. (1998) *Biochemistry 37*, 14664−14671.
43. Jiang, Y., Wilkins, P. C., and Dalton, H. (1993) *Biochim. Biophys. Acta 1163*, 105−112.
44. Gallagher, S. C., Callaghan, A. J., Zhao, J., Dalton, H., and Trewhella, J. (1999) *Biochemistry 38*, 6752−6760.
45. Rosenzweig, A. C., and Lippard, S. J. (1994) *Acc. Chem. Res. 27*, 229−236.
46. Rosenzweig, A. C., Brandstetter, H., Whittington, D. A., Nordlund, P., Lippard, S. J., and Frederick, C., A. (*1997*) *Proteins: Struct., Funct., Genet. 29*, 141−152.
47. Fisher, H. F. (1988) *Adv. Enzymol. Relat. Areas Mol. Biol. 61*, 1−41.
48. Murphy, K. P., Freire, E., and Paterson, Y. (1995) *Proteins: Struct., Funct., Genet. 21*, 83−90.
49. Walters, K. J., Gassner, G. T., Lippard, S. J., and Wagner, G. (1999) *Proc. Natl. Acad. Sci. U.S.A. 96*, 7877−7882.
50. Kazlauskaite, H., Hill, A. O., Wilkins, P. C., and Dalton, H. (1996) *Eur. J. Biochem. 241*, 552−556.
51. Paulsen, K. E., Fox, B. G., Lipscomb, J. D., Münck, E., and Stankovich, M. T. (1994) *Biochemistry 33*, 713−722.
52. Liu, K. E., and Lippard, S. J. (1991) *J. Biol. Chem. 266*, 12836−12839, 24859.
53. Raner, G. M., Martins, L. J., and Ellis, W. R., Jr. (1997) *Biochemistry 36*, 7037−7043.
54. Martins, L. J., Hill, C. P., and Ellis, W. R., Jr. (1997) *Biochemistry 36*, 7044−7049.
55. Wallar, B. J., and Lipscomb, J. D. (1996) *Chem. Rev. 96*, 2625−2657.
56. Blankenship, R. E., and Parson, W. W. (1978) *Annu. Rev. Biochem. 47*, 635−653.
57. Walker, J. E. (1992) *Q. Rev. Biophys. 25*, 253−324.
58. Gassner, G. T., Johnson, D. A., Liu, H.-w., and Ballou, D. P. (1996) *Biochemistry 35*, 7752−7761.
59. Blazyk, J. L., Gassner, G. T., and Lippard, S. J. (1998) unpublished results.

BI990841M